To appear, IEEE Trans. on
Signal Processing, march 1995.

A NEW CLASS OF TWO-CHANNEL BIORTHOGONAL FILTER BANKS AND WAVELET BASES

See-May Phoong, Student Member, IEEE, Chai W. Kim,

P. P. Vaidyanathan, Fellow, IEEE, and Rashid Ansari, Senior Member, IEEE.

Abstract: We propose a novel framework for a new class of two-channel biorthogonal filter banks. The framework covers two useful subclasses: (i) *causal stable* IIR filter banks; (ii) *linear phase* FIR filter banks. There exists a very efficient structurally perfect reconstruction implementation for such a class. Filter banks of high frequency selectivity can be achieved by using the proposed framework with low complexity. The properties of such a class are discussed in detail. The design of the analysis/synthesis systems reduces to the design of a single transfer function. Very simple design methods are given both for FIR and IIR cases. Zeros of arbitrary multiplicity at aliasing frequency can be easily imposed, for the purpose of generating wavelets with regularity property. In the IIR case, two new classes of IIR *maximally flat* filters different from Butterworth filters are introduced. The filter coefficients are given in closed form. The wavelet bases corresponding to the biorthogonal systems are generated. We also provide a novel mapping of the proposed one dimensional (1D) framework into two dimensional (2D). The mapping preserves: (i) perfect reconstruction; (ii) stability in the IIR case; (iii) linear phase in the FIR case; (iv) zeros at aliasing frequency; (v) frequency characteristic of the filters.

EDICS number: SP 2.4.3

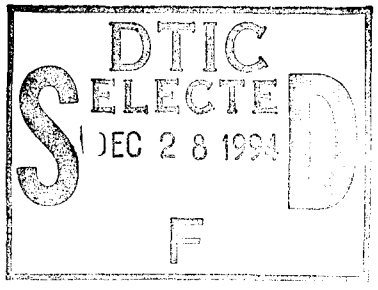

This work was supported by Office of Naval Research grant N00014-93-0231, and funds from Tektronix, Inc.

See-May Phoong and P. P. Vaidyanathan are with the Department of Electrical Engineering, California Institute of Technology, Pasadena CA 91125 USA.

Chai W. Kim is with Department of Electrical Engineering, University of Pennsylvania, 200 S. 33rd St., Philadelphia PA 19104 USA.

Rashid Ansari is with Bellcore MRE 2A-277, 445 South Street, Morristown NJ 07960 USA.

1. INTRODUCTION

Fig. 1.1(a) shows a two-channel maximally decimated filter bank, and Fig. 1.1(b) shows the well-known polyphase form for this system. The applications of such multirate systems are well-known [1]−[7]. If for all input $x(n)$, the output of the system $\hat{x}(n) = cx(n - n_0)$ for some nonzero constant c and integer n_0, the system is called a perfect reconstruction (PR) system. In the maximally decimated case, PR is equivalent to biorthogonality [5]. A number of PR or nearly PR systems have been reported before. In this paper we develop several new results for two-channel biorthogonal filter banks based on a useful class of polyphase matrices.

1.1. Previous work

In FIR filter banks, all the four filters H_0, H_1, F_0, and F_1, are FIR filters while in the case of IIR filter banks, some or all of these filters are IIR filters. The earliest good designs for the IIR case were such that the analysis bank was paraunitary and the polyphase components of $H_0(z)$ and $H_1(z)$ were allpass (see [7] or pp. 201 of [2]). Even though all the IIR filters are causal stable, the reconstructed signal suffers from phase distortion. IIR PR filter banks typically have noncausal stable filters or causal unstable filters [8], [9], [10]. Recently the authors in [11] proposed a IIR PR technique providing causal stable solutions, but no satisfactory design method was given.

In earlier design of two dimensional (2D) filter banks, separable filters have been considered because of their advantage of low complexity. However nonseparable filters offer more freedom in the design and hence in general will give better performance. Recently, some results on the nonseparable filter banks have emerged [12]−[14]. However, few design techniques are available for nonseparable PR filter banks. In [12], a design method based on space domain approach is given. In [13], a subclass of 2D paraunitary systems (which can be represented as a cascade of 1D paraunitary systems of degree one) is considered. However in both of the polyphase approaches above, the optimization in the designs involves a large number of nonlinear constraints. Thus other approaches, such as 1D to 2D mapping, have been considered [14]−[19]. In [14], even though PR property is preserved by the mapping, the frequency responses of the filters will change. In [15] and [16], a mapping of 1D filter banks to 2D filter banks is given. The authors apply the technique on a 1D two-channel orthogonal IIR system to achieve a 2D IIR filter bank. The resulting systems have either phase distortion or stability problem. In [17], the authors employ McClellan's transformation on the 1D maximally flat FIR halfband filters to obtain a 2D biorthogonal filter bank. However because of the lack of factorization theorems in the 2D case, one of the lowpass filters is constrained to have all its zeros at the aliasing frequency. And there is no simple way to ensure the frequency selectivity of all the filters. In [18], the authors introduce a mapping which can be viewed as the generalization McClellan's transformation. 2D two-channel PR systems with good frequency selectivity can be obtained by judiciously designing the

mapping. However, the mapping works for the FIR case only and the resulting filters usually have a large number of coefficients.

Some of the results in this paper were reported in the earlier conference papers [20], [21] and [22]. For the 1D case [20], both of the linear phase FIR and causal stable IIR solutions for PR filter banks similar to those proposed in this paper were given. For the 2D quincunx case [21], the authors constructed a 1D to 2D mapping (which is the same as the mapping given in Section 5 in this paper) which preserved many of the desired properties. However many of the properties of the 1D and 2D biorthogonal systems were not addressed in [20] and [21], for example the problem of imposition of zeros at the aliasing frequency which is important for the purpose of generating smooth wavelet basis functions.

1.2. The new idea and its merits

In this paper, we constrain the polyphase matrix $\mathbf{E}(z)$ such that $[\det \mathbf{E}(z)]$ is a delay. Furthermore we consider $\mathbf{E}(z)$ and $\mathbf{R}(z)$ to be either (i) both causal stable IIR or (ii) both FIR. In each case, the following properties can be simultaneously satisfied.

1. Perfect reconstruction is preserved structurally and the structural complexity is very low.
2. All analysis and synthesis filters are designed by controlling a single transfer function $\beta(z)$ [allpass in the IIR case, and Type 2 (i.e., odd order symmetric linear phase FIR) in the FIR case]. So the design procedure is very simple. It is very easy to design $\beta(z)$ so that all filters have good responses (lowpass or highpass as the case may be).
3. In the IIR case, all the analysis and synthesis filters are causal and stable.
4. In some applications such as image coding, the linear phase property of the analysis and synthesis filters is desired. In the FIR case, the filters are exact linear-phase. In the IIR case, we can force the phase response of the filters to be nearly linear in the passband, as we shall explain and demonstrate.
5. The lowpass analysis filter $H_0(z)$ can be forced to have arbitrary number of zeros at $\omega = \pi$. Furthermore the lowpass synthesis filter $F_0(z)$ is guaranteed to have the same number of zeros at π as $H_0(z)$. In both of the IIR and FIR cases, we give closed form expression for the filter coefficients that provide maximum number of zeros at π.

A new class of biorthogonal wavelet basis functions can be generated from the above filter bank. The regularity property can be directly controlled by imposing multiple zeros at π as desired. In the IIR case, since all filters are causal (in addition to being stable), the basis functions are all causal. In the FIR case, the linear phase property ensures symmetry of the wavelets, while at the same time providing a simple control on regularity (because the number of zeros at π is trivially controlled).

A 1D to 2D mapping

Furthermore, we also provide a novel mapping of the proposed 1D filter banks into the 2D quincunx

A-1

case, preserving all the desirable properties. In particular:

1. The perfect reconstruction property is preserved.
2. In the IIR case all the analysis and synthesis filters remain causal and stable. In the FIR case the linear phase property is preserved.
3. Even though the filter bank is nonseparable, the complexity is that of a separable filter bank, growing linearly with the filter order.
4. The frequency response supports for the filters are the diamond and diamond-complement as desired for the quincunx case [15], [2]. Moreover the filter frequency responses are ensured to be good simply by designing the 1D filter having a good frequency response. Any desired specifications can be met by designing a 1D transfer function $\beta(z)$ appropriately as we shall demonstrate.
5. If the 1D lowpass filter $H_0(z)$ has k zeros at π, then the resulting 2D lowpass filter will have its ith order total derivative equal to zero at (π, π), for $i = 0, 1, \ldots, k-1$. See Sec. 5 for details.

We also provide a design example to show that the mapping can be easily applied to any dilation matrix (i.e, decimation matrix) with determinant 2.

Relation to other results in the literature

All the designs proposed in this paper are based on a single class of polyphase matrices, to be described in Sec. 2. However some of the filter banks reported by other researchers are related to our work. In [23], the authors derive a class of biorthogonal linear phase FIR filter bank which turns out to be a special case of our two-channel framework. In the IIR maximally flat halfband case, our solution is different from the traditional IIR Butterworth design and has approximately linear-phase in the passband. In the FIR maximally flat halfband case, the solution agrees with the classical FIR maximally flat design [24]. But our construction is different from those in [25] and [6] since the analysis filters are factors of maximally flat halfband filters in [25] and [6] while our analysis filters are themselves maximally flat halfband. The 2D mapping proposed earlier in [15] and [16] is different from ours because it is known that the earlier mapping will not preserve the PR property in general.

1.3. Outline of the paper and notations

Our presentation will go as follows: In the next section, we will derive a framework for the two-channel biorthogonal filter banks. Some properties of such class will be described in detail. In Sec. 3, we will discuss both the IIR and FIR filter banks which are covered in the proposed framework. In Sec. 4, wavelet basis functions generated from the proposed filter banks will be presented and imposition of zeros at aliasing frequency will be considered. Two new classes of IIR maximally flat solution are given in closed form. In Sec. 5, we will first introduce a novel 2D mapping for the quincunx case. Some properties of the mapping are discussed. Then both the IIR and FIR cases are considered. Furthermore numerical examples will be

provided throughout the discussion to demonstrate the idea.

Notations and definitions: Capital boldfaced letters are used to denote matrices. **I** represents the identity matrix. The determinant of the matrix **A** is denoted by $[\det \mathbf{A}]$. Superscript ^{2D} is used to represent the 2D function obtained by applying the mapping, for example, $\mathbf{E}^{2D}(z_0, z_1)$ is obtained by applying the 2D mapping to $\mathbf{E}(z)$. The z-transform of $h(n)$ is represented by $H(z)$. The relation between the filters $\{H_k(z), F_k(z)\}$ and the polyphase matrices $\mathbf{E}(z)$ and $\mathbf{R}(z)$ can be described as follows:

$$H_k(z) = E_{k,0}(z^2) + z^{-1}E_{k,1}(z^2), \quad \text{and} \quad F_k(z) = z^{-1}R_{0,k}(z^2) + R_{1,k}(z^2),$$

where $E_{i,j}(z)$ and $R_{i,j}(z)$ are respectively the ij-th elements of the matrices $\mathbf{E}(z)$ and $\mathbf{R}(z)$. A filter $H_k(z)$ is halfband if either one of its polyphase components $E_{k,0}(z)$, $E_{k,1}(z)$ is a delay.

2. A FRAMEWORK FOR 1D BIORTHOGONAL FILTER BANKS

Consider Fig. 1.1, where a two-channel system is shown. In general, $\mathbf{R}(z) = \mathbf{E}^{-1}(z)$ for perfect reconstruction. It is not easy to constrain $[\det \mathbf{E}(z)]$ to be minimum phase for stability of $\mathbf{R}(z)$, so let us make it a delay. An example is

$$\mathbf{E}(z) = \begin{pmatrix} z^{-N} & \beta(z) \\ 0 & z^{-N'} \end{pmatrix}. \tag{2.1}$$

With this we obtain

$$H_0(z) = z^{-2N} + z^{-1}\beta(z^2), \tag{2.2}$$

but $H_1(z) = z^{-(2N'+1)}$ which is a delay. Thus even though $H_0(z)$ can be designed to be a good lowpass filter (as we will show), $H_1(z)$ is allpass and this is not useful for subband coding applications. We can modify $H_1(z)$ without affecting $H_0(z)$ by taking the polyphase matrix to be

$$\mathbf{E}(z) = \begin{pmatrix} 0.5 & 0 \\ -0.5\alpha(z) & 1 \end{pmatrix} \begin{pmatrix} z^{-N} & \beta(z) \\ 0 & z^{-N'} \end{pmatrix} = \begin{pmatrix} 0.5z^{-N} & 0.5\beta(z) \\ -0.5z^{-N}\alpha(z) & -0.5\alpha(z)\beta(z) + z^{-N'} \end{pmatrix}. \tag{2.3}$$

Then we get the following expressions for the analysis filters:

$$H_0(z) = \frac{(z^{-2N} + z^{-1}\beta(z^2))}{2}, \quad H_1(z) = -\alpha(z^2)H_0(z) + z^{-2N'-1}. \tag{2.4}$$

Obtaining ideal responses with (2.4)

First notice that the filter $H_0(z)$ can be made an ideal lowpass filter if $\beta(z)$ has the following magnitude and phase responses:

$$|\beta(e^{j2\omega})| = 1, \qquad \forall\, \omega \tag{2.5a}$$

$$\angle\beta(e^{j2\omega}) = \begin{cases} (-2N+1)\omega, & \text{for } \omega \in [0, \pi/2]; \\ (-2N+1)\omega \pm \pi, & \text{for } \omega \in (\pi/2, \pi]. \end{cases} \tag{2.5b}$$

From (2.4), we see that in the high frequency region, $H_1(e^{j\omega})$ has unity gain since $|H_0(e^{j\omega})| = 0$. The function $\alpha(z)$ does not affect $H_0(z)$ and can be freely chosen to shape the response of $H_1(z)$. It should

be chosen such that in the low frequency region, $\alpha(z^2)H_0(z)$ cancels with $z^{-2N'-1}$. For exact magnitude cancellation, $|\alpha(e^{j\omega})|$ must be unity. Since $H_0(z)$ is linear phase, it is necessary that $\alpha(z)$ has linear phase in the low frequency region. Comparing these two requirements and the conditions in (2.5), we realize that $\beta(z)$ is a suitable candidate for $\alpha(z)$. Indeed, if $N' = 2N-1$, $H_1(z)$ is an ideal highpass filter. In this case, we have an ideal filter bank, and the polyphase matrix $\mathbf{E}(z)$ in Fig. 1.1(b) is

$$\mathbf{E}(z) = \begin{pmatrix} 0.5 & 0 \\ -0.5\beta(z) & 1 \end{pmatrix} \begin{pmatrix} z^{-N} & \beta(z) \\ 0 & z^{-2N+1} \end{pmatrix} = \begin{pmatrix} 0.5z^{-N} & 0.5\beta(z) \\ -0.5z^{-N}\beta(z) & -0.5\beta^2(z) + z^{-2N+1} \end{pmatrix}. \tag{2.6}$$

With this we get the following expressions for the analysis filters, which we will repeatedly use in this paper.

$$H_0(z) = \frac{(z^{-2N} + z^{-1}\beta(z^2))}{2}, \quad H_1(z) = -\beta(z^2)H_0(z) + z^{-4N+1}. \tag{2.7}$$

The perfect reconstruction can be achieved by choosing $\mathbf{R}(z)$ in Fig. 1.1(b) to be:

$$\mathbf{R}(z) = \begin{pmatrix} z^{-2N+1} & -\beta(z) \\ 0 & z^{-N} \end{pmatrix} \begin{pmatrix} 1 & 0 \\ 0.5\beta(z) & 0.5 \end{pmatrix} = \begin{pmatrix} z^{-2N+1} - 0.5\beta^2(z) & -0.5\beta(z) \\ 0.5z^{-N}\beta(z) & 0.5z^{-N} \end{pmatrix}. \tag{2.8}$$

The corresponding synthesis filters can be verified to have the following form:

$$F_0(z) = -H_1(-z), \quad F_1(z) = H_0(-z). \tag{2.9}$$

This choice of synthesis filters in (2.9) ensures that $\{F_0(z), F_1(z)\}$ is a lowpass/highpass pair if $\{H_0(z), H_1(z)\}$ is a lowpass/highpass pair. From (2.6) and (2.8), we have the implementation of the filter bank shown in Fig. 2.1. The structure is similar to a ladder network structure [26].

Remarks: Of course, the $\alpha(z)$ in (2.3) can be taken as functions different from $\beta(z)$, as in the case of [20], [21], [23]. This will provide more freedom in the design. However, by taking them to be the same, the biorthogonal systems can have some additional useful properties. Therefore, we will only consider the case when $\alpha(z) = \beta(z)$.

Two useful approximations of (2.5)

The ideal choice of $\beta(z)$ as in (2.5) requires infinite complexity. Therefore, we have to design $\beta(z)$ to approximate the conditions in (2.5). However the approximation will not change the perfect reconstruction property because $\mathbf{E}(z)$ in (2.6) and $\mathbf{R}(z)$ in (2.8) satisfy $\mathbf{R}(z)\mathbf{E}(z) = 0.5z^{-3N+1}\mathbf{I}$, regardless of the choice of $\beta(z)$. Fig. 2.1 shows that the frequency responses of all the analysis and synthesis filters depend on one single function $\beta(z)$ only. The frequency selectivity of all four filters depends on how well $\beta(z)$ approximates conditions (2.5). This makes the design procedure simple. In the next section, we will provide two simple but useful approximations which correspond to the following two cases:

1. *Stable IIR case:* Here $\beta(z)$ is chosen to be a causal stable allpass function so that (2.5a) is met exactly. We design the phase response of the allpass filter so that (2.5b) is approximately satisfied. This leads to a biorthogonal system with *causal stable* IIR analysis and synthesis filters.

2. *Linear phase FIR case:* To satisfy the condition (2.5b), $\beta(z)$ can be chosen as a Type 2 linear phase function [2] (filter with a symmetric impulse response of even length). The magnitude response of $\beta(z)$ is optimized to be as close to unity as possible so that (2.5a) is well-approximated. This leads to a *linear phase* biorthogonal system.

Additional properties of the filter banks designed as above

In Sec. 1, we have outlined some properties. Properties $1-4$ mentioned at the begining of Sec 1.2 are clear from the above discussion and Property 5 will be discussed in the Sec. 4. In addition to these five properties, we have

1. *Double halfband property:* In all the previous constructions of two-channel PR filter banks, $H_0(z)F_0(z)$ is a halfband filter, where $H_0(z)$ is not necessary halfband but a factor of a halfband filter. However in our construction above, one can verify that not only the product $H_0(z)F_0(z)$ but also the filter $H_0(z)$ is halfband.
2. *Poles of filters:* In the IIR case, notice from Fig. 2.1 that there is no feedback loop in both the analysis and synthesis ends in the ladder network. Therefore the filters have the same poles as those of $\beta(z^2)$ and stability depends solely on the allpass function $\beta(z)$. Moveover in the IIR case if the allpass filter $\beta(z)$ is implemented by using the robust lattice structure [2], the filter bank is stable even when it is realized with finite wordlength.
3. *Robustness to round off noise:* The ladder structure shown in Fig. 2.1 is similar to the structure considered in [26]. By using the same reasoning in [26], it can be verified that the round off noise in the analysis end is compensated by that in the synthesis end. Combining this with the structurally PR property, we conclude that the implementation in Fig. 2.1 preserves PR even when all the coefficients are quantized to a finite percision and all the intermediate results are rounded off. However, if the subband signals are quantized (which is usually the case), this property is lost.
4. *Zeros of the filters:* We can verify that $F_0(z)$ and $H_1(z)$ in (2.9) and (2.7) can respectively be rewritten as:

$$F_0(z) = \big(2z^{-2N+1} - \beta(z^2)\big)H_0(z), \quad H_1(z) = \big(2z^{-2N+1} + \beta(z^2)\big)F_1(z). \tag{2.10}$$

These factorizations give the filter bank an interesting structure shown in Fig. 2.2. From (2.10), it is clear that if $\beta(z)$ is FIR, the zeros of $H_0(z)$ are also zeros of $F_0(z)$. Even when $\beta(z)$ is an irreducible IIR transfer function, this is true since $H_0(z)$ is in the form of (2.7) and the zeros of denominator of $\beta(z^2)$ cannot cancel the zeros of $H_0(z)$. Moreover if $|\beta(e^{j\omega})| < 2$, both $F_0(e^{j\omega})$ and $H_0(e^{j\omega})$ have the same set of zeros on the unit circle. The same is true for the pair of $H_1(z)$ and $F_1(z)$. In particular, if $H_0(z)$ has r zeros at $z = -1$, this implies that $F_0(z)$ has no fewer than r zeros at the same point. This property is important in the generation of wavelets since for biorthogonal wavelets, we need both of the analysis

and the synthesis wavelets to be regular. By increasing the number of zeros of $H_0(z)$ at $z = -1$, our construction ensures that $F_0(z)$ has at least the same number of zeros at $z = -1$. This is the property which does not appear in the previously existing constructions of biorthogonal filter banks.

5. *Ripple sizes of the filters:* Since $H_0(z)$ is a halfband filter and $H_0(z) + F_1(z) = z^{-2N}$, we have the following relationship between the passband ripple δ_p and the stopband ripple δ_s:

$$\delta_p(H_0) = \delta_s(H_0) = \delta_p(F_1) = \delta_s(F_1). \tag{2.11}$$

Moreover by using (2.10) and the fact that $\beta(z^2) \approx -z^{-2N+1}$ in the high frequency region, we get

$$\delta_s(F_0) \approx 3\delta_s(H_0), \quad \delta_s(H_1) \approx 3\delta_s(F_1), \tag{2.12}$$

($20 \log 3 \approx 9.5$ dB). This property ensures that by designing $H_0(z)$ to have sufficiently high stopband attenuation, we can ensure that all the other three filters will also have good frequency selectivity.

6. *Complexity:* From Fig. 2.1, it is very clear that the analysis and synthesis banks have the same complexity. Assume that $\beta(z)$ has order N. For the IIR case, by using the one multiplier lattice structure for allpass function [2], we need approximately $2N$ multiplications, $6N$ additions, and $5N$ delays. For the FIR case, by exploiting the symmetry, we need approximately N multiplications, $2N$ additions and $3.5N$ delays. All the operations are at a lower rate. So the analysis (or synthesis) bank requires N and $0.5N$ multiplications per input sample for the IIR and FIR case respectively.

7. *Near linear phase in the IIR cases:* From (2.7), since in the passband the magnitude response of $H_0(z)$ is approximately one, the transfer function $\beta(z^2) \approx z^{-2N+1}$. Therefore $H_0(z)$ has approximately linear phase in the passband. Similar arguement is true for $H_1(z)$.

3. DESIGN PROCEDURES FOR THE TWO CLASSES OF BIORTHOGONAL FILTER BANKS

In this section, we will discuss the two cases of the approximations of (2.5) given in the last section. Simple design procedures will be given for both cases.

3.1. Causal Stable IIR Biorthogonal Filter Banks

In this section, $\beta(z)$ in (2.6)−(2.9) is taken to be the causal stable real allpass function

$$A_{N_1}(z) = \frac{\sum_{k=0}^{N_1} a_{N_1,N_1-k} z^{-k}}{\sum_{k=0}^{N_1} a_{N_1,k} z^{-k}}, \tag{3.1}$$

where $a_{N_1,0} = 1$ and $a_{N_1,k}$ are real. In this case, $H_0(z)$ is a sum of a delay and an allpass function. See Eq. (2.7). It is an IIR halfband filter and has been studied by some researchers [27], [28]. $H_0(z)$ can be made lowpass with large stopband attenuation and small passband ripples by designing the phase response of the allpass function to approximate (2.5b) [29].

Choice of N_1: From the monotone decreasing phase property [2] of a causal stable allpass function, we know that the phase of $A_{N_1}(z^2)$ spans a range of $4N_1\pi$ when ω spans a range of 2π. But from (2.5b), $\beta(z^2)$ spans a range of $4N\pi$ or $4(N-1)\pi$. To make the range spanned by both of the functions equal, we set $N_1 = N$ or $N-1$ and this results in two classes of causal stable IIR filter banks. Since the derivation and properties of both of the classes are very similar, in the rest of the paper, we consider only the case $N_1 = N$ (we will point out at those places where the second class has a different property). With this choice, the analysis filters can be written as

$$H_0(z) = \frac{(z^{-2N} + z^{-1}A_N(z^2))}{2}, \quad H_1(z) = -A_N(z^2)H_0(z) + z^{-4N+1}. \tag{3.2}$$

The relationship between the synthesis and analysis filters is the same as (2.9).

Additional properties of the above IIR filter banks:

1. *Preservation of zero at aliasing frequency:* Substituting $z = -1$ into the expression of $H_0(z)$ in (3.2), we find that $H_0(z)$ always have a zero at $z = -1$, independent of the coefficients $a_{N,k}$. In particular, the zero is preserved even when all $a_{N,k}$ are quantized coarsely. This means that one zero at $z = -1$ is structurally imposed. This is important in the generation of wavelet bases since one zero at $z = -1$ is a necessary condition for the existence of the wavelet functions [6]. Note also that $H_1(z)$ will always have a structurally imposed zero at $z = 1$.
2. *Low sensitivity:* Since there exists low sensitivity lattice structure for allpass function [2], the filters have low passband sensitivity. Since the halfband property of $H_0(z)$ is structurally imposed, it has low stopband sensitivity as well.
3. *Bump in the transition band:* Substituting $\omega = \pi/2$ into the expression for $H_1(e^{j\omega})$ and $F_0(e^{j\omega})$ and using the fact that $A_N(-1) = (-1)^N$, we find that $|H_1(e^{j\omega})| = |F_0(e^{j\omega})| = \sqrt{2.5}$ at $\omega = \pi/2$, independent of the allpass function $A_N(z)$. This means that $|H_1(e^{j\omega})|$ and $|F_0(e^{j\omega})|$ always have a bump of approximately 4 dB at $\omega = \pi/2$, no matter how we design $A_N(z)$. The width but not amplitude of the bump can be reduced by increasing the complexity of $A_N(z)$.

Example 3.1 1D causal stable IIR filter banks: In this example, $N = 3$. So $A_N(z)$ is a third order allpass function. The filter bank has very low complexity: To implement the analysis (or synthesis) bank, we need only 3 multiplications per input sample! By using the eigenfilter approach for allpass functions [29] we optimize the coefficients a_k such that maximum attenuation in the stopband of $H_0(z)$ is achieved. The coefficients are obtained as $a_{3,1} = 0.473$, $a_{3,2} = -0.094$, and $a_{3,3} = 0.025$. For the filter $H_0(z)$, the passband edge $\omega_p = 0.4\pi$ and the stopband egde $\omega_s = 0.6\pi$. The stopband attenuation $\delta_s(H_0) = 41.9$ dB. The magnitude responses of the all four filters are shown in Fig. 3.1(a). From the plots, relations of ripple sizes in (2.11) and (2.12) can be verified and it is clear that $H_0(z)$ and $F_0(z)$ have the same set of zeros on the unit circle. The bump of approximately 4 dB around $\pi/2$ is clearly seen. The group delay for $H_0(z)$ and

$H_1(z)$ is shown in Fig. 3.1(b). The filters are approximately linear phase in the passband and the stopband.

3.2. Linear Phase FIR Biorthogonal Filter Banks

In the linear phase FIR case, since $H_0(z)$ is a linear phase halfband filter, it can be designed by employing the trick developed in [30], viz, by taking $\beta(z)$ in (2.5)−(2.8) to be a Type 2 filter [2] which has a symmetric impulse response of length $2N_1$. In this case, the number of multiplications required to implement $\beta(z)$ is N_1, the same as the N_1th order allpass function $A_{N_1}(z)$ in (3.1). More precisely, let $\beta(z)$ have the following form:

$$V(z) = \sum_{k=1}^{N_1} v_k \times (z^{-N_1+k} + z^{-N_1-k+1}), \tag{3.3}$$

where the coefficients v_k satisfy:

$$\sum_{k=1}^{N_1} v_k = 0.5, \tag{3.4}$$

so that $V(e^{j0}) = 1$ and $H_0(e^{j0}) = 1$. It is well-known that a Type 2 linear phase filter always has a zero at $z = -1$. In order to satisfy the condition (2.5b) exactly, it can be verified that N_1 should be equal to N. By employing the trick in [30], the coefficients v_k can be optimized such that the amplitude response of $V(e^{j\omega})$ is as close to unity as possible. In this case, the analysis filters are:

$$H_0(z) = \frac{(z^{-2N} + z^{-1}V(z^2))}{2}, \quad H_1(z) = -V(z^2)H_0(z) + z^{-4N+1}. \tag{3.5}$$

Example 3.2. 1D linear phase FIR filter banks: $N = 6$. To implement the analysis bank, we need 6 multiplications per input sample, double the number in Example 3.1. The Type 2 linear phase function $V(z)$ is designed by using McClellan-Park algorithm. The coefficients are obtained as $v_1 = 0.630$, $v_2 = -0.193$, $v_3 = 0.0972$, $v_4 = -0.0526$, $v_5 = 0.0272$ and $v_6 = -0.0144$. For the filter $H_0(z)$, the passband edge $\omega_p = 0.4\pi$ and the stopband edge $\omega_s = 0.6\pi$, same condition as Example 3.1. The stopband attenuation $\delta_s(H_0) = 39.2$ dB and $\delta_s(H_1) = 30$ dB. The magnitude responses of all four filters are shown in Fig. 3.2. The relations of ripple sizes in (2.11) and (2.12) can be verified.

For comparison, we will consider Johnston's design with nearly the same specifications. The Johnston's filter 24C in Appendix 7.1 of [31] has $\delta_s = 30$ dB and $\omega_s = 0.586\pi$. For Johnston's filter 32D, $\delta_s = 38$ dB and $\omega_s = 0.586\pi$. To implement the analysis bank, we need respectively 12 multiplications and 16 multiplications per input sample for the above two cases. Thus as compared to 6 multiplications in our filter bank, the Johnston's design has more complexity than our design. Moreover, there is reconstruction error (0.1 dB for 24C and 0.025 dB for 32D) in Johnston's filter bank.

4. IMPOSITION OF MULTIPLE ZEROS AT π

The relation between continuous-time wavelet and discrete-time perfect reconstruction filter bank is well known. A way to construct the scaling and wavelet functions from the filter coefficients was first given by

Daubechies in [6]. Starting from the impulse response coefficients $h_0(n)$ and $h_1(n)$, a pair of continuous-time functions $\phi_{H_0}(x)$ and $\psi_{H_1}(x)$ are constructed such that they satisfy:

$$\phi_{H_0}(x) = \sum_{n=0}^{\infty} h_0(n)\phi_{H_0}(2x-n), \tag{4.1a}$$

$$\psi_{H_1}(x) = \sum_{n=0}^{\infty} h_1(n)\phi_{H_0}(2x-n). \tag{4.1b}$$

Here $\phi_{H_0}(x)$ and $\psi_{H_1}(x)$ are respectively called the analysis scaling and wavelet functions. For the synthesis end, we can write similar expressions for the synthesis scaling and wavelet functions, $\phi_{F_0}(x)$ and $\psi_{F_1}(x)$. The conditions for the existence of such limit functions were given in [6]. It is always desirable to have smooth or "regular" limit functions. It was shown that in order to achieve limit functions of high regularity, we need to have a sufficient number of zeros at the aliasing frequency π. Therefore in the rest of this section, we will show how to impose zeros at π for the proposed filter banks.

4.1. Causal Stable IIR Wavelet Bases

For the purpose of achieving regularity, we impose multiple zeros of $H_0(z)$ at π. Since the denominator does not provide any zeros, we consider only the numerator of $H_0(z)$. Except for a delay, the numerator of $H_0(z)$ can be written in terms of $a_{N,k}$ as follows:

$$P_R(\omega) = \sum_{k=0}^{N} a_{N,k}\cos(2k-1/2)\omega. \tag{4.2}$$

To obtain r zeros at $z=-1$, we set

$$P_R^{(i)}(\pi) \triangleq \frac{d^{(i)}}{d\omega^{(i)}} P_R(\omega)\Big|_{\omega=\pi} = 0, \quad \text{for } i = 1,\ 2,\ \ldots,\ r-1. \tag{4.3}$$

Note that when i is even, $P_R^{(i)}(\pi)$ is always equal to zero. This proves that $P_R(\omega)$ always has an *odd* number of zeros at $\omega=\pi$. Therefore, we can write $r = 2r_0+1$. In this case, we obtain a set of r_0 linear constraints as follows:

$$\sum_{k=0}^{N} a_{N,k}(1-4k)^{2i-1} = 0, \text{ for } i = 1,\ 2,\ \ldots,\ r_0. \tag{4.4}$$

The set of linear constraints in (4.4) can be satisfied *exactly* in the optimization of the phase response of the allpass function $A_N(z)$ by using the efficient eigenfilter approach [29], [32].

Maximally flat IIR wavelets

To obtain a maximally flat solution, i.e., maximum possible number of zeros at π consistent with the constraint that $H_0(z) = 0.5(z^{-2N}+z^{-1}A_N(z^2))$, we set r_0 in (4.4) as large as possible. However if $r_0 \geq N+1$, then we can list the first $(N+1)$ linear constraints given by (4.4) as follows:

$$\underbrace{\begin{pmatrix} 1 & 1 & \cdots & 1 \\ x_0^2 & x_1^2 & \cdots & x_N^2 \\ \vdots & \vdots & \ddots & \vdots \\ x_0^{2N} & x_1^{2N} & \cdots & x_N^{2N} \end{pmatrix}}_{Vandermonde} \begin{pmatrix} x_0 & & & \\ & x_1 & & \\ & & \ddots & \\ & & & x_N \end{pmatrix} \begin{pmatrix} a_{N,0} \\ a_{N,1} \\ \vdots \\ a_{N,N} \end{pmatrix} = \begin{pmatrix} 0 \\ 0 \\ \vdots \\ 0 \end{pmatrix}, \tag{4.5}$$

where $x_k = 1 - 4k$. Since all the x_k are nonzero and distinct, the two matrices on the left hand side are nonsingular and hence invertible. We get $[a_{N,0}\, a_{N,1} \ldots a_{N,N}]^T = \mathbf{0}$ which violates the requirement that $a_{N,0} = 1$. This proves under the constraint that $H_0(z) = 0.5[z^{-2N} + z^{-1}A_N(z^2)]$, the filter $H_0(z)$ can have at most $2N+1$ zeros at π. Indeed we can show that the maximally flat IIR filter has *exactly* $2N+1$ zeros at π. To see this, we set $r_0 = N$ and rewrite the set of N linear equations given by (4.4) as follows:

$$\begin{pmatrix} 1 & 1 & \cdots & 1 \\ x_1^2 & x_2^2 & \cdots & x_N^2 \\ \vdots & \vdots & \ddots & \vdots \\ x_1^{2N-2} & x_2^{2N-2} & \cdots & x_N^{2N-2} \end{pmatrix} \begin{pmatrix} x_1 & & & \\ & x_2 & & \\ & & \ddots & \\ & & & x_N \end{pmatrix} \begin{pmatrix} a_{N,1} \\ a_{N,2} \\ \vdots \\ a_{N,N} \end{pmatrix} = - \begin{pmatrix} 1 \\ 1 \\ \vdots \\ 1 \end{pmatrix}, \tag{4.6}$$

where $x_k = 1 - 4k$ and the fact that $a_{N,0} = 1$ has been imposed. These equations fully determine $A_N(z)$ (hence all the filters) and there is no further parameter to be optimized numerically. As the matrices are invertible, the solution for $a_{N,k}$ always exists and it is *unique*. Furthermore, it is shown in Appendix A that $a_{N,k}$ has the following closed form solution:

$$a_{N,k} = \frac{(-1)^{k-1}}{2k-1} \binom{N}{k} \prod_{i=1}^{N} \frac{(2i-1)}{(2k+2i-1)}, \quad 0 \le k \le N, \tag{4.7}$$

where $\binom{N}{k} = \frac{N!}{(N-k)!k!}$. The frequency responses of $H_0(z)$ corresponding to $N = 1,\ 3,\ \cdots,\ 10$ are shown in Fig. 4.1. Note that although these filters have a numerator of degree $4N-1$ (excluding the trivial delay factor), they have only $2N+1$ zeros at $z = -1$. This implies that some of the zeros are not at $z = -1$ for $N > 1$ and therefore these IIR maximally flat filters are different from the Butterworth halfband filters. Moreover they have nearly linear phase in the passband, as justified at the end of Sec. 2 and demonstrated in Fig. 3.1(b). For the case of $N = 1$, one can verify that the solution is a third order Butterworth filter.

Remarks:

1. If the function $\beta(z)$ is taken as $(N-1)$th order allpass filter (i.e. $N_1 = N-1$), then we will get a second class of causal stable IIR wavelet. In this case, under the constraint that $H_0(z) = 0.5[z^{-2N} + z^{-1}A_{N-1}(z^2)]$, the process of imposition of zeros at π is very similar to the derivation above. The maximally flat IIR filter $H_0(z)$ of this second class will have $2N-1$ zeros at π. The closed form solution for $a_{N-1,k}$ is given as:

$$a_{N-1,k} = \frac{(-1)^{k-1}}{2k+1} \binom{N-1}{k} \prod_{i=1}^{N-1} \frac{(2i+1)}{(2k+2i+1)}, \quad 1 \le k \le N-1, \tag{4.8}$$

   and $a_{N-1,0} = 1$.

2. Notice that for a perfect reconstruction system, if we interchange the analysis and synthesis filters, the perfect reconstruction property is retained. In many applications such as coding, compression, storage and approximation, the regularity of the synthesis functions is more important [17]. Thus we can choose the wavelet with higher regularity among $\psi_{H_0}(x)$ and $\psi_{F_0}(x)$ as the synthesis wavelet.

Example 4.1. We generate the limit functions, ϕ_{H_0}, ψ_{H_1}, ϕ_{F_0}, and ψ_{F_1}, corresponding to the filter bank in Fig. 1.1(a). To generate the analysis/synthesis scaling and wavelet functions, we use the cascade algorithm in [6] for eight iterations. We consider the following two cases

(i) No linear constraint is set, $H_0(z)$ has only one zero at π. The analysis and synthesis filters are the same as those in Example 3.1. For the analysis bank, the scaling and wavelet functions, ϕ_{H_0} and ψ_{H_1}, are respectively shown in Fig. 4.2(a) and (b). The scaling and wavelet functions corresponding to the synthesis bank, ϕ_{F_0} and ψ_{F_1}, are shown in Fig. 4.2(c) and (d).

(ii) As a comparison, we also generate the scaling and wavelet functions corresponding to the IIR maximally flat filters (ϕ_{max} and ψ_{max}) for $N = 3$. In this case, the filter $H_0(z)$ has seven zeros at π. The limit functions are shown in Fig. 4.3. For a better comparison on smoothness, in Fig. 4.4 we show a zoom-in for Fig. 4.2(a) and Fig. 4.3(a). We see that the limit functions in Fig. 4.3 are more regular than the functions shown in Fig. 4.2.

4.2. Linear phase FIR wavelet bases

To impose multiple zeros at π for the linear phase FIR case, the procedure is very similar to that given above. Another set of linear constraints can be obtained and incorporated in the procedure of optimization. It can be verified that for this case, $H_0(z)$ always has an *even* number of zeros at π.

Maximally flat linear phase FIR wavelets

The FIR maximally flat filters have been studied by a number of researchers [24], [33], [6], [25]. In [6] and [25], a maximally flat halfband FIR filter is used to construct compactly supported maximally flat wavelets. In our linear phase FIR filter bank, if all the freedom is used to impose zeros at π, we will arrive at the same solution as that in [6] and [25]. The closed form solution for FIR maximally flat halfband filters was in [33], [25] as:

$$v_k = \frac{(-1)^{N+k-1}\prod_{i=0}^{2N}(N+1/2-i)}{2(N-k)!(N-1+k)!(2k-1)}. \tag{4.9}$$

Differences between our construction and those in [25], [6]: In [25], $H_0(z)$ is taken to be a factor of a maximally flat halfband filter. In [6], power spectral factorization is considered. However, in our linear phase structure, $H_0(z)$ is taken to be this halfband filter itself, and not a factor. Since the $H_0(z)$ constructed in [6] is a power spectral factor of the $H_0(z)$ in our structure, our linear phase scaling function $\phi_{LP}(x)$ is related to that constructed by Daubechies in [6], $\phi_D(x)$ as:

$$\phi_{LP}(x) = \phi_D(x) * \phi_D^*(-x), \tag{4.10}$$

where $*$ denotes convolution and ϕ_D^* denotes the complex conjugate of ϕ_D. From (4.10), it is clear that the regularity of $\phi_{LP}(x)$ is twice that of $\phi_D(x)$. However the order (and the number of zeros at π) of $H_0(z)$ in our construction is twice that of $H_0(z)$ in the construction in [6]. Comparing the complexity, both of the

constructions have approximately the same number of multiplications (because in our construction, linear phase property can be exploited).

Example 4.2. In this example, we construct the limit functions corresponding to the filter bank in Fig. 1.1(a) for the linear phase FIR case. The cascade algorithm is used for eight iterations. We consider two cases

(i) First, $H_0(z)$ is designed such that no linear constraint other than (3.4) is satisfied, therefore it has two zeros at π. The analysis and synthesis filters are the same as those in Example 3.2. The limit functions (ϕ_{H_0}, ψ_{H_1}, ϕ_{F_0} and ψ_{F_1}) are respectively shown in Fig. 4.5(a), (b), (c) and (d).

(ii) For a comparison, we show the limit functions of the maximum flat case (ϕ_{max} and ψ_{max}) for $N = 6$. In this case, $H_0(z)$ has twelve zeros at π. The plots are shown in Fig. 4.6. It can be verified that the limit functions in Fig. 4.6 are smoother than those in Fig. 4.5.

5. MAPPING INTO 2D QUINCUNX PERFECT RECONSTRUCTION FILTER BANKS

In this section, we will generalize the 1D framework discussed in Sec. 2 to the 2D case. We will focus on the quincunx subsampling case which has the subsampling lattice shown in Fig. 5.1. Notice that the dilation matrix has determinant 2. The corresponding maximally decimated filter bank has only two channels. Furthermore it represents the simplest nonseparable subsampling lattice.

In the 2D case, we know that the desired passband supports of the filters depend not only on the lattice but also on the choice of dilation matrix $\mathbf{M}$ [12]. In the rest of this section, we will consider

$$\mathbf{M} = \begin{pmatrix} 1 & 1 \\ 1 & -1 \end{pmatrix}. \tag{5.1}$$

The coset vectors are respectively:

$$\mathbf{k}_0 = \begin{pmatrix} 0 \\ 0 \end{pmatrix}, \quad \mathbf{k}_1 = \begin{pmatrix} 1 \\ 0 \end{pmatrix}. \tag{5.2}$$

With this $\mathbf{M}$, the ideal supports for alias free decimation, $SPD(\pi \mathbf{M}^{-T})$ [Chapter 12, 2] is shown in Fig. 5.2, where the diamond and diamond-complement, Ω_0 and Ω_1, correspond to the low frequency and high frequency regions respectively. One can verify that $\mathbf{M}$ defined in (5.1) has its eigenvalues λ_i equal to $\pm\sqrt{2}$ and $\mathbf{M}^2 = 2\mathbf{I}$. It has a dilation in both the directions. Therefore, $\mathbf{M}$ satisfies the conditions for a *well-behaved* matrix defined in [19]. Given the dilation matrix $\mathbf{M}$ as in (5.1) and the coset vectors in (5.2), the simple delay chain system and the noble identities are shown in Fig. 5.3(a) and (b) respectively.

Although the discussion in this paper is mainly on the quincunx subsampling case with the dilation matrix $\mathbf{M}$ and the coset vectors $\mathbf{k}_i$ defined above, we will provide a design example in the last section to show that the method discussed in this section can be easily generalized to any 2D system with decimation matrix $\mathbf{M}$ having $[\det \mathbf{M}] = 2$.

5.1. A 1D to 2D Mapping

In this subsection, we will first give a 2D mapping and then apply the mapping to the framework developed in Sec. 2. Given any 1D biorthogonal systems with the polyphase matrices of the form in (2.6) and (2.8), we will use the following transformation on the polyphase components:

(i) First replace the 1D transfer function $\beta(z)$ with the separable 2D transfer function $\beta(z_0)\beta(z_1)$.

(ii) Replace all the remaining 1D delay z^{-1} with the 2D delay $z_0^{-1}z_1^{-1}$.

This results in nonseparable analysis and synthesis filters as we will see. Under this transformation, the polyphase matrices $\mathbf{E}^{2D}(z_0, z_1)$ and $\mathbf{R}^{2D}(z_0, z_1)$ of the 2D system can be written respectively as:

$$\begin{aligned}\mathbf{E}^{2D}(z_0,z_1) &= \begin{pmatrix} 0.5 & 0 \\ -0.5\beta(z_0)\beta(z_1) & 1 \end{pmatrix} \begin{pmatrix} (z_0z_1)^{-N} & \beta(z_0)\beta(z_1) \\ 0 & (z_0z_1)^{-2N+1} \end{pmatrix} \\ &= \begin{pmatrix} 0.5(z_0z_1)^{-N} & 0.5\beta(z_0)\beta(z_1) \\ -0.5(z_0z_1)^{-N}\beta(z_0)\beta(z_1) & -0.5\beta^2(z_0)\beta^2(z_1) + (z_0z_1)^{-2N+1} \end{pmatrix}. \end{aligned} \tag{5.3}$$

$$\begin{aligned}\mathbf{R}^{2D}(z_0,z_1) &= \begin{pmatrix} (z_0z_1)^{-2N+1} & -\beta(z_0)\beta(z_1) \\ 0 & (z_0z_1)^{-N} \end{pmatrix} \begin{pmatrix} 1 & 0 \\ 0.5\beta(z_0)\beta(z_1) & 0.5 \end{pmatrix} \\ &= \begin{pmatrix} (z_0z_1)^{-2N+1} - 0.5\beta^2(z_0)\beta^2(z_1) & -0.5\beta(z_0)\beta(z_1) \\ 0.5(z_0z_1)^{-N}\beta(z_0)\beta(z_1) & 0.5(z_0z_1)^{-N} \end{pmatrix}. \end{aligned} \tag{5.4}$$

From the above two equations, we have the implementation of the 2D perfect reconstruction filter bank as Fig. 5.4. By using the noble identities in Fig. 5.3, we can write the analysis and synthesis filters as:

$$\begin{aligned} H_0(z_0,z_1) &= \frac{z_0^{-2N} + z_0^{-1}\beta(z_0z_1^{-1})\beta(z_0z_1)}{2}, \\ H_1(z_0,z_1) &= -\beta(z_0z_1^{-1})\beta(z_0z_1)H_0(z_0,z_1) + z_0^{-4N+1}, \end{aligned} \tag{5.5a}$$

$$F_0(z_0,z_1) = -H_1(-z_0,-z_1), \qquad F_1(z_0,z_1) = H_0(-z_0,-z_1). \tag{5.5b}$$

Comparison of the above transformation with those in [15] – [17]: McClellan's transformation is used in [17] to obtain a FIR maximally flat halfband filter. The transformation proposed in this paper differs from McClellan's transformation in the sense that the former operates on the polyphase components while the latter operates directly on the filter. In [15] and [16], the authors obtain a 2D filter bank from 1D by employing the following transformation:

$$\mathbf{E}_{i,j}^{2D}(z_0,z_1) = \mathbf{E}_{i,j}(z_0)\mathbf{E}_{i,j}(z_1), \tag{5.6}$$

where $\mathbf{E}_{i,j}$ is the (i,j)th element of $\mathbf{E}$. It is clear that in our transformation $\mathbf{E}_{1,1}^{2D}(z_0,z_1) \neq \mathbf{E}_{1,1}(z_0)\mathbf{E}_{1,1}(z_1)$. Therefore our mapping is different from that in (5.6).

Properties of the proposed 2D mapping

Properties 1–5 in Sec. 2 continue to hold after minor modifications to suit the 2D context. In addition, the 2D filter bank satisfies the following properties

1. *Double halfband property:* It is easy to see that $H_0(z_0, z_1)$ satisfies $H_0(z_0, z_1) + H_0(-z_0, -z_1) = z_0^{-2N}$ and $H_0(z_0, z_1)F_0(z_0, z_1)$ satisfies a similar property. This is the extention of the 1D double halfband property in the 2D quincunx case.

2. *Stability of the 2D analysis and synthesis filters:* If the 1D transfer function $\beta(z)$ is causal then so are the functions $\beta(z_0)\beta(z_1)$ in Fig. 5.4. That is $\beta(z_0)\beta(z_1)$ is a first-quadrant filter (the impulse response is zero unless $n_0 \geq 0$ and $n_1 \geq 0$). If $\beta(z)$ is BIBO stable, then so is $\beta(z_0)\beta(z_1)$ so that the polyphase matrix in Fig. 5.4 is also BIBO stable. Since the analysis filters are obtained from this stable structure, these filters are guaranteed to be BIBO stable. However we see that the term $\beta(z_0 z_1^{-1})$ has entered the expressions for the analysis filters because of the noble identities, see Fig. 5.3(b). It can be shown that this violates the condition for the so-called first-quadrant stability (p. 166 of [35]). This is explained by the fact that the analysis filters are *not* first-quadrant filters, even though BIBO stable. This is consistent with the observation that the quincunx decimator $\mathbf{M}$ in (5.1) has the negative entry -1. Indeed, the expression $y(\mathbf{n}) = x(\mathbf{Mn})$ means $y(n_0, n_1) = x(n_0 + n_1, n_0 - n_1)$ so that there is a time-reversal operation buried in the decimation process. The same remarks apply for the synthesis filters, that is the 2D synthesis filters $F_0(z_0, z_1)$ and $F_1(z_0, z_1)$ are BIBO stable even though they are not first-quadrant filters.

3. Perfect reconstruction is preserved.

4. If the 1D lowpass filter $H_0(z)$ has k zeros at π, then the frequency response of $H_0(e^{j\omega_0}, e^{j\omega_1})$ can be written as

$$H_0(e^{j\omega_0}, e^{j\omega_1}) = \left(1 + e^{-j\frac{\omega_0+\omega_1}{2}}\right)^k P_1(\omega_0, \omega_1) - \left(1 + e^{-j\frac{\omega_0-\omega_1+2\pi}{2}}\right)^k P_2(\omega_0, \omega_1), \tag{5.7}$$

where $|P_1(\pi, \pi)|$ and $|P_2(\pi, \pi)|$ are finite quantities. The proof of (5.7) is given in Appendix B. Notice that both of the factors $[1 + e^{-0.5j(\omega_0+\omega_1)}]$ and $[1 + e^{-0.5j(\omega_0-\omega_1+2\pi)}]$ are zero at (π, π). Furthermore one can verify that all the mixed partial derivatives satisfy

$$\frac{\partial^{i+l}}{\partial\omega_0^i \partial\omega_1^l} H_0(e^{j\omega_0}, e^{j\omega_1})\Big|_{(\pi,\pi)} = 0, \quad \text{for } i + l < k. \tag{5.8}$$

From (5.8), we conclude that the total derivatives [36]

$$d^n H_0(\pi, \pi) = \sum_{i=0}^{n} \binom{n}{i} d\omega_0^i d\omega_1^{n-i} \frac{\partial^n}{\partial\omega_0^i \partial\omega_1^{n-i}} H_0(\pi, \pi) = 0, \quad \text{for } n < k. \tag{5.9}$$

According to [34], (5.9) is a necessary condition for the regularity of 2D wavelet. The necessary and sufficient condition is still unknown.

5. In the FIR case the linear phase property of the analysis and synthesis filters is preserved.

6. In the IIR case, the 2D analysis and synthesis filters have a line of zeros in the frequency plane at $\omega_0 = 0$ or at $\omega_0 = \pi$.

   Proof: Substituting $z_0 = -1$ into the expression for $H_0(z_0, z_1)$ in (5.5a) and using the fact that $\beta(z_0 z_1)$ is allpass, one immediately finds that $H_0(-1, z_1) = 0, \ \forall \ z_1$. Since $F_0(z_0, z_1)$ contains $H_0(z_0, z_1)$ as a factor, $F_0(-1, z_1) = 0$. Similarly, we can prove that $F_1(1, z_1) = H_1(1, z_1) = 0, \ \forall \ z_1$.

7. The lowpass/highpass characteristics of the frequency responses of the filters are preserved.

   Proof: Assume that $\beta(z)$ satisfies the ideal conditions in (2.5). Then we have

$$\beta(z_0 z_1) = \begin{cases} (z_0 z_1)^{\frac{-2N+1}{2}}, & \text{for } \frac{\omega_0+\omega_1}{2} \in [0, \pi/2]; \\ -(z_0 z_1)^{\frac{-2N+1}{2}}, & \text{for } \frac{\omega_0+\omega_1}{2} \in (\pi/2, \pi]. \end{cases} \tag{5.10a}$$

$$\beta(z_0 z_1^{-1}) = \begin{cases} (z_0 z_1^{-1})^{\frac{-2N+1}{2}}, & \text{for } \frac{\omega_0-\omega_1}{2} \in [0, \pi/2]; \\ -(z_0 z_1^{-1})^{\frac{-2N+1}{2}}, & \text{for } \frac{\omega_0-\omega_1}{2} \in (\pi/2, \pi]. \end{cases} \tag{5.10b}$$

   By using the above equations, we find that $\beta(z_0 z_1)\beta(z_0 z_1^{-1})$ is equal to z_0^{-2N+1} when $(\omega_0, \omega_1) \in \Omega_0$ and equal to $-z_0^{-2N+1}$ when $(\omega_0, \omega_1) \in \Omega_1$. This proves that $H_0(z_0, z_1)$ has the ideal diamond support Ω_0. Similarly it can be shown that $H_1(z_0, z_1)$ will have the support of ideal diamond-complement. Thus when the conditions in (2.5) are well-approximated by the 1D transfer function $\beta(z)$, the response of the 2D filters will be good.

Comments on the complexity: Though the 2D analysis and synthesis filters are nonseparable, it is clear from the expressions for the polyphase matrices that the complexity is comparable to that of a separable filter bank. More precisely, it is equal to twice the complexity of the 1D transfer function $\beta(z)$.

5.2. 2D Nonseparable Filter Banks

In this section, we will give two numerical examples to demonstrate the mapping proposed above. We separately apply the 2D mapping to the filter banks in Example 3.1 (IIR) and Example 3.2 (FIR) respectively.

Example 5.1. 2D IIR filter banks: In this example, we transform the 1D filter bank in Example 3.1 into the 2D case by using above mapping. Since $N = 3$, the allpass function $A_3(z)$ needs only 3 multiplications. Since the complexity of the 2D analysis (or synthesis) bank is equal to twice that of $A_3(z)$, we need only 6 multiplications per input pixel to implement the analysis (synthesis) bank. The responses of $H_0(z_0, z_1)$ and $H_1(z_0, z_1)$ are shown in Fig. 5.5(a) and (b) respectively. The supports of the two filters are diamond and diamond-complement respectively as desired. The stopband attenuation $\delta_s(H_0) \approx 42$ dB and $\delta_s(H_1) \approx 32$ dB. Again, we see that H_1 is about 10 dB worse than H_0 in the stopband. The line of zero of H_1 at $\omega_0 = 0$ is clearly seen in Fig. 5.5(b).

Example 5.2. 2D FIR filter banks: In this example, the 1D filter bank in Example 3.2 is transformed into the 2D case. To implement the 2D analysis (or synthesis) bank, we need 12 multiplications per input

pixel. The magnitude responses of $H_0(z_0, z_1)$ and $H_1(z_0, z_1)$ are shown in Fig. 5.6(a) and (b) respectively. The stopband attenuation $\delta_s(H_0) \approx 40$ dB and $\delta_s(H_1) \approx 30$ dB.

6. CONCLUDING REMARKS

In this paper, we have derived a framework for a new class of two-channel biorthogonal filter banks. The filter banks under the framework allow a structurally perfect reconstruction implementation as in Fig. 2.1. It is interesting that we can arrive at precisely the same ladder in Fig. 2.1 by using the novel approach in [26] developed for a totally different application, namely cancellation of roundoff error. The proposed systems have very low complexity. Filter banks of high frequency selectivity can be achieved by controlling a single transfer function $\beta(z)$ in Fig. 2.1. Two different choices of $\beta(z)$ lead to causal stable IIR and linear phase FIR filter banks respectively. The properties of the proposed filter banks were discussed in detail. We showed that zeros at aliasing frequency can be imposed. Two new types of IIR maximally flat filters were derived and the solutions were given in closed form. In addition to perfect reconstruction property, these IIR filters have nearly linear phase in the passband. Furthermore, we also mapped the 1D filter banks derived in this paper into 2D cases. The design of a 2D biorthogonal (stable IIR or linear phase FIR) filter bank reduces to the design of a single 1D transfer function. The new transformation preserves many of the properties of the 1D systems. Before we conclude the paper, we would like to provide an example to demonstrate that the mapping in Sec. 5 can be easily generalized to arbitrary dilation matrix $\mathbf{M}$ with determinant equal to 2.

Example 6.1. 2D IIR filter banks: The 1D prototype filter bank is taken to be that in Example 3.1. The dilation matrix and the coset vectors are respectively:

$$\mathbf{M} = \begin{pmatrix} 3 & 1 \\ 1 & 1 \end{pmatrix}, \quad \mathbf{k_0} = \begin{pmatrix} 0 \\ 0 \end{pmatrix} \quad \mathbf{k_1} = \begin{pmatrix} 2 \\ 1 \end{pmatrix}. \tag{6.1}$$

With the above matrix and coset vectors, the ideal passband support for the $H_0(z_0, z_1)$ is $SPD(\pi \mathbf{M}^{-T})$, which is shown in Fig. 6.1 (shaded area). By using the tranformation introduced in Sec. 5, we find that the polyphase matrices in this example are the same as those in Example 5.1. Thus it also has very low complexity. The only differences are the dilation matrix and the coset vectors. With the $\mathbf{M}$ and $\mathbf{k_i}$ chosen as (6.1), the responses of $H_0(z_0, z_1)$ and $H_1(z_0, z_1)$ are shown in Fig. 6.1(a) and (b). We see that H_0 and H_1 have approximately the desired support.

Appendix A. Proof of Eq. (4.7)

It is shown in [33] that there exists closed form solution for $a_{N,k}$ satisfying system of linear equations:

$$1+\sum_{k=1}^{N} a_{N,k} x_k^{2r} = 0, \quad \text{for } r = 1,\ 2,\ \ldots,\ N. \tag{A.1}$$

With some modification, the solution to (4.6) can be written as:

$$a_{N,k} = -\frac{1}{x_k} \prod_{i=1}^{k-1} \frac{1-x_{k-i}^2}{x_k^2 - x_{k-i}^2} \prod_{j=k+1}^{N} \frac{x_j^2 - 1}{x_j^2 - x_k^2}, \tag{A.2}$$

where $x_k = 1 - 4k$. Substituting the value for x_k into the equation, we find that

$$\prod_{i=1}^{k-1} \frac{1-x_{k-i}^2}{x_k^2 - x_{k-i}^2} = (-1)^{k-1} \prod_{i=1}^{k-1} \frac{(2i-1)}{(4k-2i-1)}, \tag{A.3a}$$

$$\prod_{j=k+1}^{N} \frac{x_j^2 - 1}{x_j^2 - x_k^2} = \binom{N}{k} \prod_{j=k+1}^{N} \frac{(2j-1)}{(2k+2j-1)}. \tag{A.3b}$$

Combining (A.3a) and (A.3b), we get (4.7).

Appendix B. Proof of Property 4 in Section 5.1

Supposing that the 1D filter $H_0(z)$ has k zeros at π, then we have

$$e^{j\omega} H_0(e^{j\omega}) = e^{(-2N+1)j\omega} + \beta(e^{2j\omega}) = \left(1 + e^{j\omega}\right)^k p(e^{j\omega}), \tag{B.1}$$

where $|p(-1)|$ is a finite nonzero constant. From (5.6a), we have

$$e^{j\omega_0} H_0(e^{j\omega_0}, e^{j\omega_1}) = e^{(-2N+1)j\omega_0} + \beta(e^{j(\omega_0+\omega_1)})\beta(e^{j(\omega_0-\omega_1)}). \tag{B.2}$$

From (B.2), $e^{j\omega_0} H_0(e^{j\omega_0}, e^{j\omega_1})$ can be rewritten as

$$\begin{aligned} e^{j\omega_0} H_0(e^{j\omega_0}, e^{j\omega_1}) =& \beta(e^{j(\omega_0-\omega_1)}) \left(e^{(-2N+1)j\frac{\omega_0+\omega_1}{2}} + \beta(e^{j(\omega_0+\omega_1)}) \right) \\ & - e^{(-2N+1)j\frac{\omega_0+\omega_1}{2}} \left(\beta(e^{j(\omega_0-\omega_1)}) - e^{(-2N+1)j\frac{\omega_0-\omega_1}{2}} \right). \end{aligned} \tag{B.3}$$

By using (B.1) and the fact that $\beta(e^{j\omega})$ is of period 2π, we get (5.7).

Acknowledgement

The authors would like to thank Dr. Tsuhan Chen of AT&T Bell Labs, and Igor Djokovic, graduate student of California Institute of Technology, Pasadena, for fruitful discussions. Dr. Chen also provided the software for the allpass design using the eigenfilter approach for Example 3.1.

References

[1] M. J. T. Smith, and T. P. Barnwell, "A new filter-bank theory for time-frequency representation," *IEEE Trans. on Acoustics, Speech and Signal Proc.*, pp. 314-327, March 1987.

[2] P. P. Vaidyanathan, *Multirate systems and filter banks*, Englewood Cliffs, NJ: Prentice Hall, 1993.

[3] P. P. Vaidyanathan, "Multirate digital filters, filter banks, polyphase networks, and applications: a tutorial," *Proc. of the IEEE*, vol 78, pp. 56-93, Jan. 1990.

[4] M. Vetterli, "A theory of multirate filter banks," *IEEE Trans. on Acoustics, Speech and Signal Proc.*, pp. 356-372, Mar. 1987.

[5] P. P. Vaidyanathan, "Orthonormal and biorthonormal filter-banks as convolvers, and convolutional coding gain," *IEEE Trans. on Signal Processing*, vol. 41, pp. 2210-2231, June 1993.

[6] I. Daubechies, "Orthonormal bases of compactly supported wavelets," *Commun. Pure Appl. Math.*, vol. 41, pp. 909-996, Nov. 1988.

[7] P. P. Vaidyanathan, P. Regalia, and S. K. Mitra, "Design of doubly complementary IIR filters using a single complex allpass filter, with multirate applications," *IEEE Trans. on Circuits and Systems*, vol. 34, pp. 378-389, April 1987.

[8] T. A. Ramstad, "IIR filter bank for subband coding of images," *Proc. IEEE Int. Symp. Circuits and Systems*, pp. 827-830, Espoo, Finland, 1988.

[9] C. Herley, and M. Vetterli, "Wavelets and recursive filter banks," *IEEE Trans. on Signal Proc.*, vol. 41, no. 8, pp. 2536-56, Aug. 1993.

[10] S. K. Mitra, C. D. Creusere, and H. Babic, "A novel implementation of perfect reconstruction QMF banks using IIR filters for infinite length signals," *Proc. IEEE Int. Symp. on Circuits and Systems,* pp. 2312-15, San Diego, May 1992.

[11] S. Basu, C.-H. Chiang, and H. M. Choi, "Wavelets and perfect reconstruction subband coding with causal stable IIR filters," *preprint.*

[12] E. Viscito, and J. Allebach, " Design of perfect reconstruction multidimensional filter banks using cascaded Smith form matrices," *Proc. IEEE Int. Symp. on Circuits and Systems,* Espoo, Finland, pp. 831-834, June 1988.

[13] G. Karlsson, and M. Vetterli, "Theory of two-dimensional multirate filter banks," *IEEE Trans. Acoustics, Speech and Signal Proc.*, vol. 38, pp. 925-937, June 1990.

[14] I. A. Shah, and A. A. C. M. Kalker, "Generalized theory of multidimensional M-band filter bank design," *Proc. of the Sixth EUSIPCO,* pp. 969-972, Aug. 1992.

[15] R. Ansari, and C.-L. Lau, "Two-dimensional IIR filters for exact reconstruction in tree-structured subband decomposition," *Electronics letters,* vol. 23, pp. 633-634, June 1987.

[16] T. Chen, and P. P. Vaidyanathan, "Multidimensional multirate filters and filter banks derived from one-dimensional filters," *IEEE Trans. on Signal Proc.*, vol. 41, no. 5, pp. 1749-65, May 1993.

[17] A. Cohen, and I. Daubechies, "Non-separable bidimensional wavelet bases," *preprint.*

[18] B. H. Tay, and N. G. Kingsbury, "Flexible design of multidimensional perfect reconstruction FIR 2-band

filters using transformations of variables," *IEEE Trans. on Image Proc.,* vol. 2, no. 4, pp. 466-480, Oct. 1993.

[19] J. Kovacevic, and M. Vetterli, "Nonseparable multidimensional perfect reconstruction filter banks and wavelet bases for R^n," *IEEE Trans. Information Theory,* vol. 38, no. 2, pp. 533-555, Mar. 1992.

[20] C. W. Kim, and R. Ansari, " FIR/IIR exact reconstruction filter banks with applications to subband coding of images," *Proc. of Midwest CAS Symp.,* Monterey, CA, May 1991.

[21] C. W. Kim, and R. Ansari, "Subband decomposition procedure for quincunx sampling grids," *Proc. of SPIE-Visual Comm. and Image Proc.,* Boston, MA, Nov 1991.

[22] S.-M. Phoong, and P. P. Vaidyanathan, "Two-channel 1D and 2D biorthonormal filter banks with causal stable IIR and linear phase FIR filters," *Proc. IEEE Int. Symp. on Circuits and Systems,* London, England, May 1994.

[23] H. Kiya, M. Yae, and M. Iwahashi, "A linear phase two-channel filter bank allowing perfect reconstruction," *Proc. IEEE Int. Symp. Circuits and Systems,* pp. 951-954, San Diego, 1992.

[24] O. Herrmann, "On the approximation problem in nonrecursive digital filter design," *IEEE Trans. Circuit Theory,* vol. 18, pp. 411-413, May 1971.

[25] R. Ansari, C. Guillemot, and J. F. Kaiser, "Wavelet construction using Lagrange halfband filters," *IEEE Trans. Circuits and Systems,* vol. 38, no. 9, pp. 1116-1118, Sep. 1991.

[26] A. M. Bruekers, and Ad W. M. van den Enden, "New networks for perfect inversion and perfect reconstruction," *IEEE Jour. Selected Areas in Communication,* vol. 10, no. 1, pp. 130-137, Jan. 1992.

[27] R. Ansari, and B. Liu, "Efficient sampling rate alteration using recursive (IIR) digital filters," *IEEE Trans. Acoustics, Speech and Signal Proc.,* vol. 31, pp. 1366-73, Dec. 1983.

[28] M. Renfors, and T. Saramaki, "Recursive Nth-band digital filters–part I: Design and properties," *IEEE Trans. Circuits and Systems,* vol. 34, no. 1, pp. 24-39, Jan. 1987.

[29] T. Q. Nguyen, T. I. Laakso, and R. D. Koilpillai, "Eigenfilter approach for the design of allpass filters approximating given phase response," *preprint.*

[30] P. P. Vaidyanathan, and T. Q. Nguyen, "A "TRICK" for the design of FIR half-band filters," *IEEE Trans. Circuits and Systems,* vol. 34, no. 3, pp. 297-300, Mar. 1987.

[31] R. E. Crochiere, and L. R. Rabiner, *Multirate digital signal processing,* Englewood Cliffs, NJ: Prentice Hall, 1983.

[32] T. Chen, and P. P. Vaidyanathan, "Design of IFIR eigenfilters," *Proc. IEEE Int. Symp. on Circuits and Systems,* pp. 264-267 Singapore 1991.

[33] C. Gumacos, "Weighting coefficients for certain maximally flat nonrecursive digital filters," *IEEE Trans. Circuits and Systems,* vol. 25, no. 4, pp. 234-235, Apr. 1978.

[34] I. Daubechies, private communication.

[35] N. K. Bose, *Applied multidimensional systems theory,* New York NY: Van Nostrand Reinhold, 1982.

[36] S. Lang, *Calculus of several variables,* New York NY: Springer-Verlag, 1987.

LIST OF FIGURES

Fig. 1.1. (a) A two-channel analysis/synthesis filter bank. (b) A redrawing of (a) by using the polyphase representation.

Fig. 2.1. An implementation of the proposed biorthogonal filter bank.

Fig. 2.2. A redrawing of Fig. 2.1, where $H_0(z) = 0.5(z^{-2N} + z^{-1}\beta(z^2))$, and $F_1(z) = H_0(-z)$.

Fig. 3.1. (Example 3.1) Frequency responses of the causal stable IIR filter bank. (a) Magnitude responses of the analysis and synthesis filters. (b) Group delays of $H_0(z)$ and $H_1(z)$.

Fig. 3.2. (Example 3.2) Magnitude responses of the linear phase FIR filter bank.

Fig. 4.1. Magnitude responses of the IIR maximally flat filters of the form $0.5[z^{-2N} + z^{-1}A_N(z^2)]$ where $A_N(z)$ is a Nth order allpass function, for $N = 1, 2, \ldots, 10$.

Fig. 4.2. (Example 4.1(i)) The limit functions generated by using the IIR filter bank in Example 3.1 ($H_0(z)$ has one zero at π). (a) Analysis scaling function. (b) Analysis wavelet function. (c) Synthesis scaling function. (d) Synthesis wavelet function.

Fig. 4.3. (Example 4.1(ii)) The limit functions generated by using the IIR maximally flat filter bank ($H_0(z)$ has 7 zeros at π). (a) Analysis scaling function. (b) Analysis wavelet function. (c) Synthesis scaling function. (d) Synthesis wavelet function.

Fig. 4.4. A zoom-in for Fig. 4.2(a) and Fig. 4.3(a) demonstrating the improved "regularity" obtained by imposing zeros at π.

Fig. 4.5. (Example 4.2(i)) The symmetric limit functions generated by using the FIR filter bank in Example 3.2 ($H_0(z)$ has 2 zeros at π). (a) Analysis scaling function. (b) Analysis wavelet function. (c) Synthesis scaling function. (d) Synthesis wavelet function.

Fig. 4.6. (Example 4.2(ii)) The symmetric limit functions generated by using the FIR maximally flat filter bank ($H_0(z)$ has 12 zeros at π). (a) Analysis scaling function. (b) Analysis wavelet function. (c) Synthesis scaling function. (d) Synthesis wavelet function.

Fig. 5.1. The quincunx subsampling lattice.

Fig. 5.2. Ideal supports for alias-free decimation in quincunx case.

Fig. 5.3. Some details for the quincunx decimator. (a) The delay chain perfect reconstruction system, and (b) the noble identities.

Fig. 5.4. A 2D biorthogonal filter bank obtained from Fig. 2.1 by mapping.

Fig. 5.5. (Example 5.1) Magnitude responses of the perfect reconstruction IIR analysis bank. (a) $H_0(z_0, z_1)$ and (b) $H_1(z_0, z_1)$. The normalized frequency $f_i = \omega_i/2\pi$.

Fig. 5.6. (Example 5.2) Magnitude responses of the perfect reconstruction FIR analysis bank. (a) $H_0(z_0, z_1)$ and (b) $H_1(z_0, z_1)$.

Fig. 6.1. The ideal supports for alias-free decimation for $\mathbf{M}$ defined in (6.1).

Fig. 6.2. (Example 6.1) Magnitude responses of the perfect reconstruction analysis bank with the decimator $\mathbf{M}$ defined in (6.1). (a) $H_0(z_0, z_1)$ and (b) $H_1(z_0, z_1)$.

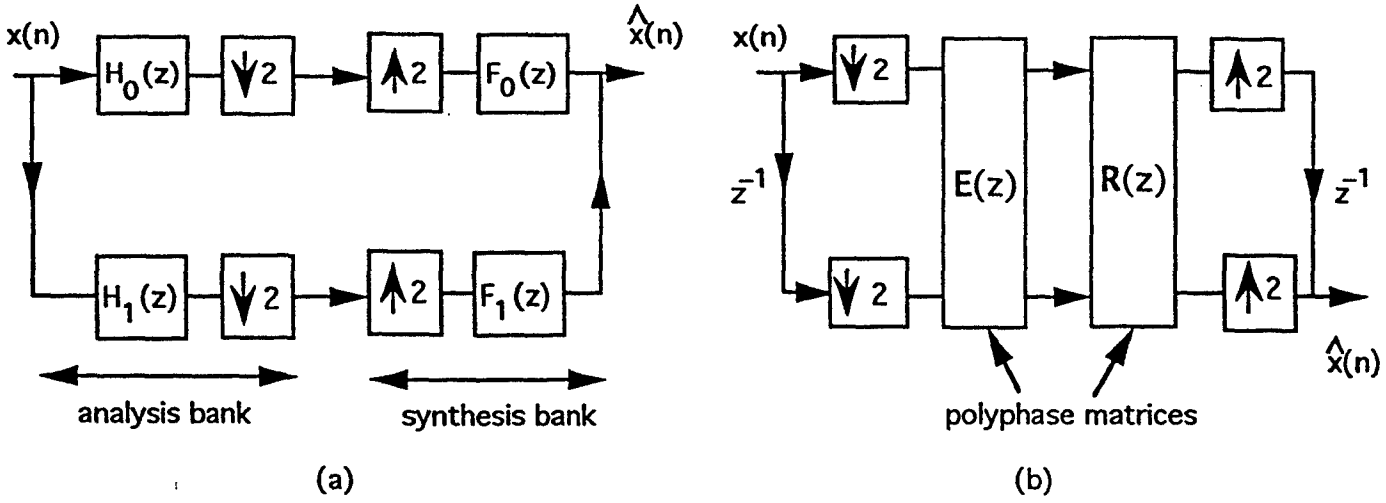

Fig. 1.1 (a) A two-channel analysis/synthesis filter bank.
(b) A redrawing of (a) by using the polyphase representation.

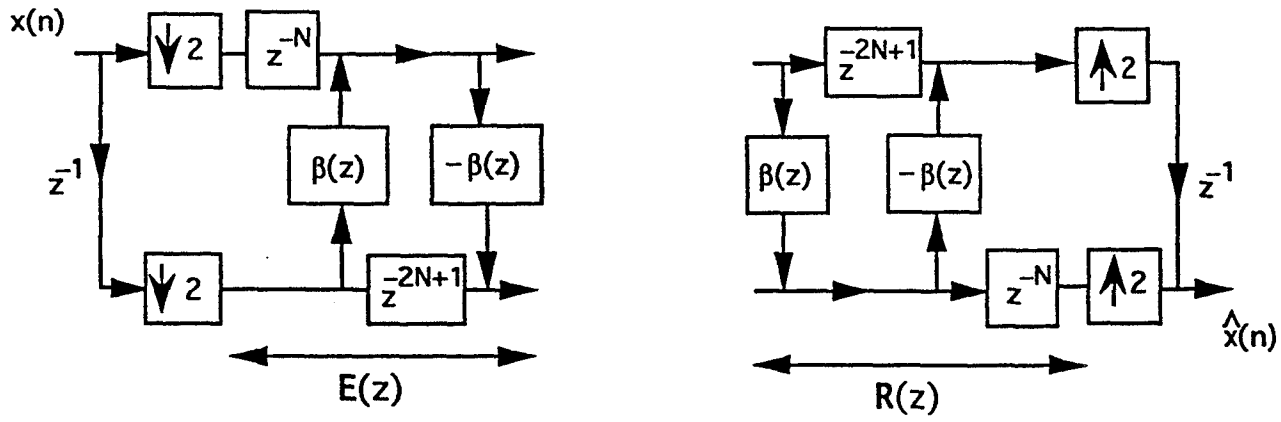

Fig. 2.1. An implementation of the proposed biorthogonal filter bank.

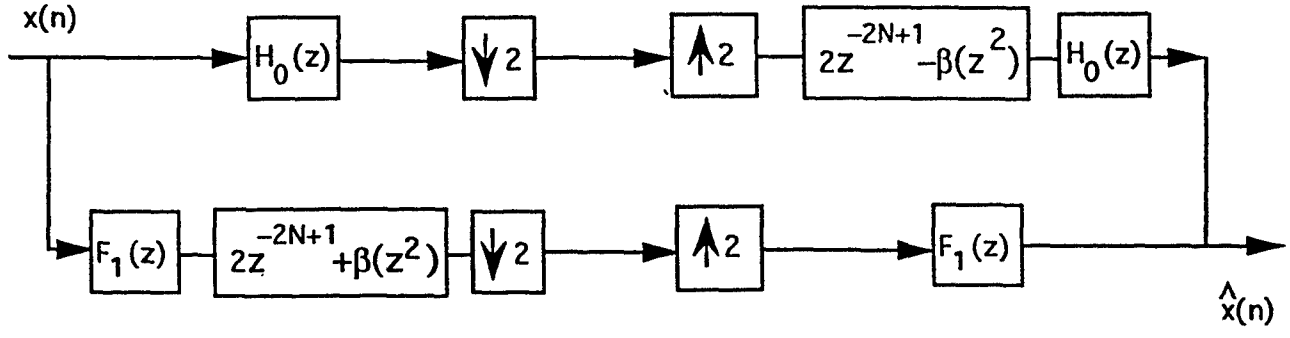

Fig. 2.2. A redrawing of Fig. 2.1, where
$H_0(z) = \frac{z^{-2N_1}+z^{-1}\beta(z^2)}{2}$, $F_1(z) = H_0(-z)$.

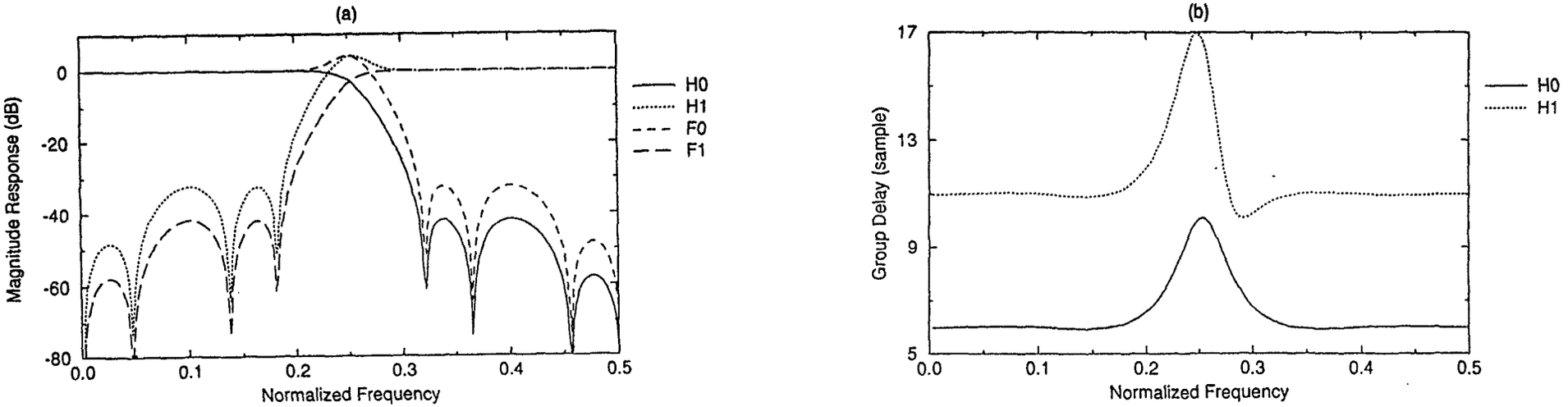

Fig. 3.1. (Example 3.1) Frequency responses of the causal stable IIR filter bank.
(a) Magnitude responses of the analysis and synthesis filters.
(b) Group delays of $H_0(z)$ and $H_1(z)$.

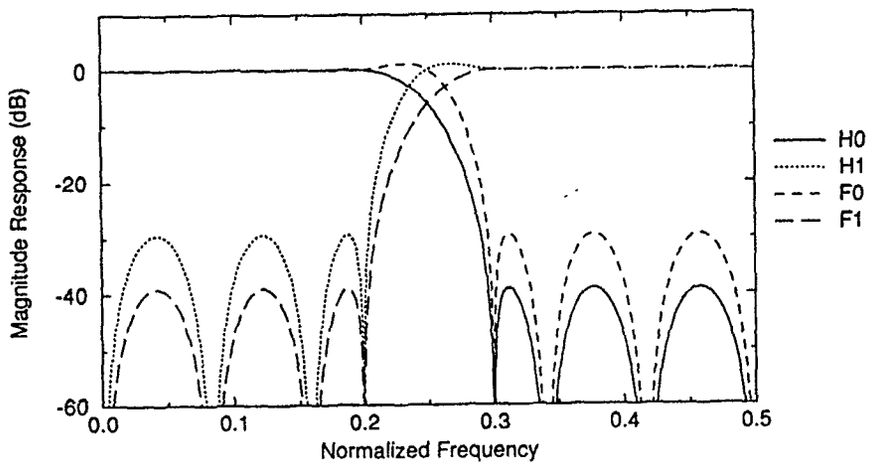

Fig. 3.2. (Example 3.2) Magnitude responses of the linear phase FIR filter bank.

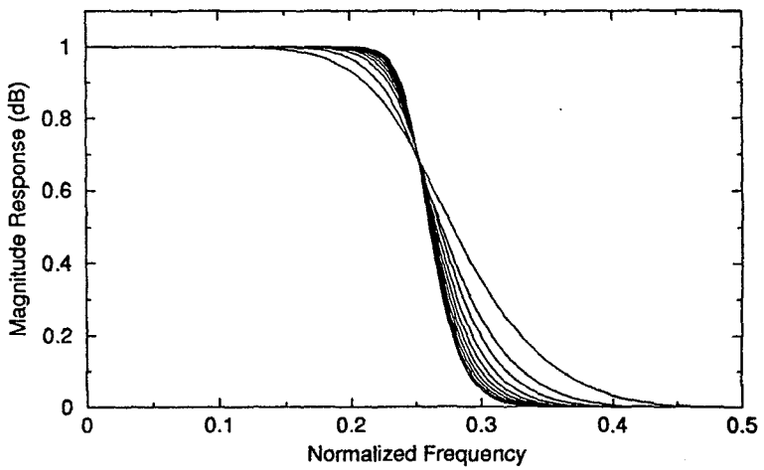

Fig. 4.1. Magnitude responses of the IIR maximally flat filters of the form $0.5\ [\ z^{-2N} + z^{-1}\ A_N\ (z^2\ )]$ where $A_N\ (z)$ is a Nth order allpass function, for N=1, 2, ..., 10.

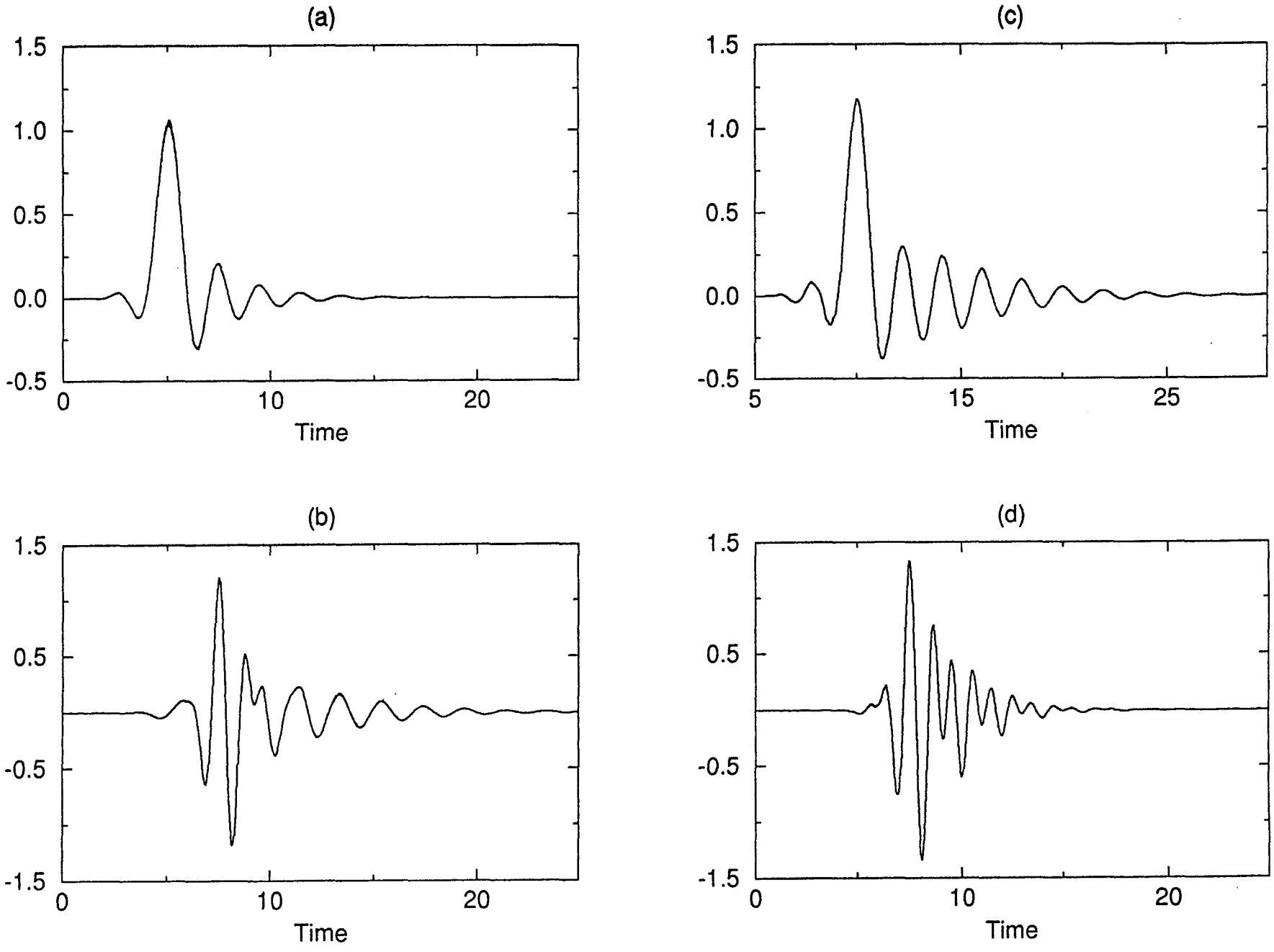

Fig. 4.2. (Example 4.1(i)) The limit functions generated by using the IIR filter bank in Example 3.1 ($H_0(z)$ has 1 zero at π).
(a) Analysis scaling function. (b) Analysis wavelet function.
(c) Synthesis scaling function. (d) Synthesis wavelet function.

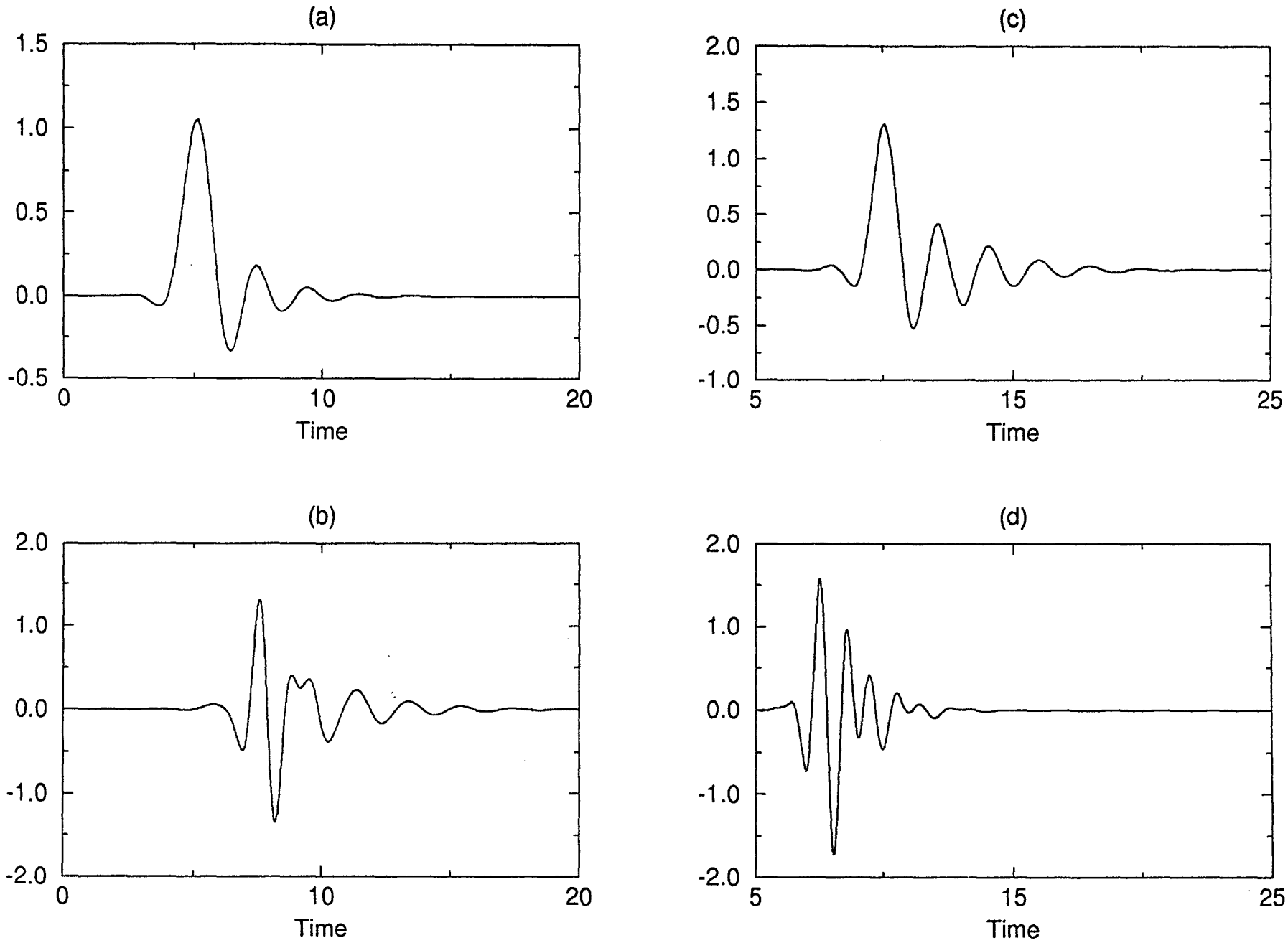

Fig. 4.3. (Example 4.1(ii)) The limit functions generated by using the IIR maximally flat filter bank ($H_0(z)$ has 7 zeros at π).
(a) Analysis scaling function. (b) Analysis wavelet function.
(c) Synthesis scaling function. (d) Synthesis wavelet function.

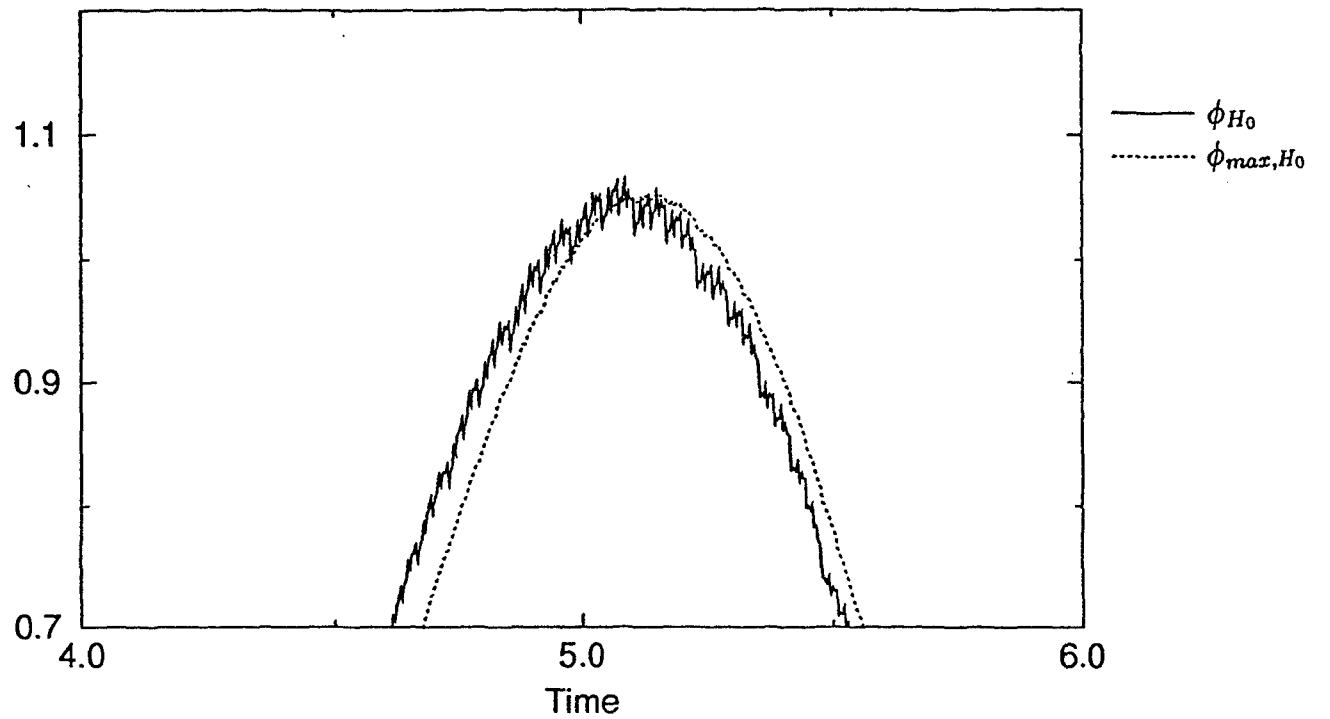

Fig. 4.4. A zoom-in for Fig. 4.2(a) and Fig. 4.3(a) demonstrating the improved "regularity" obtained by imposing zeros at π.

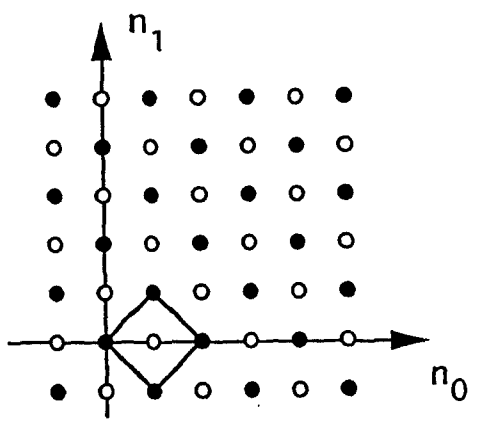

Fig. 5.1. The quincunx subsampling lattice.

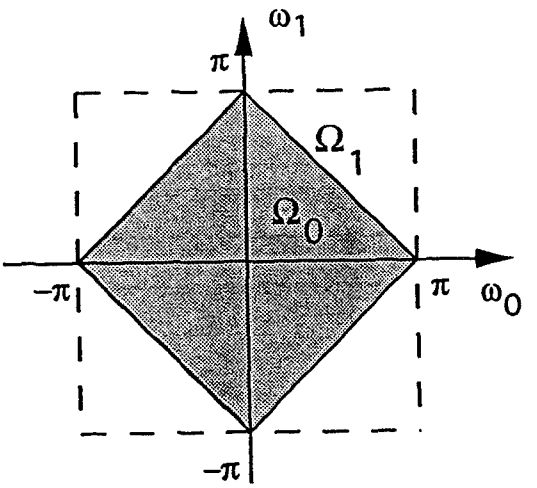

Fig. 5.2. Ideal supports for alias-free decimation in quincunx case.

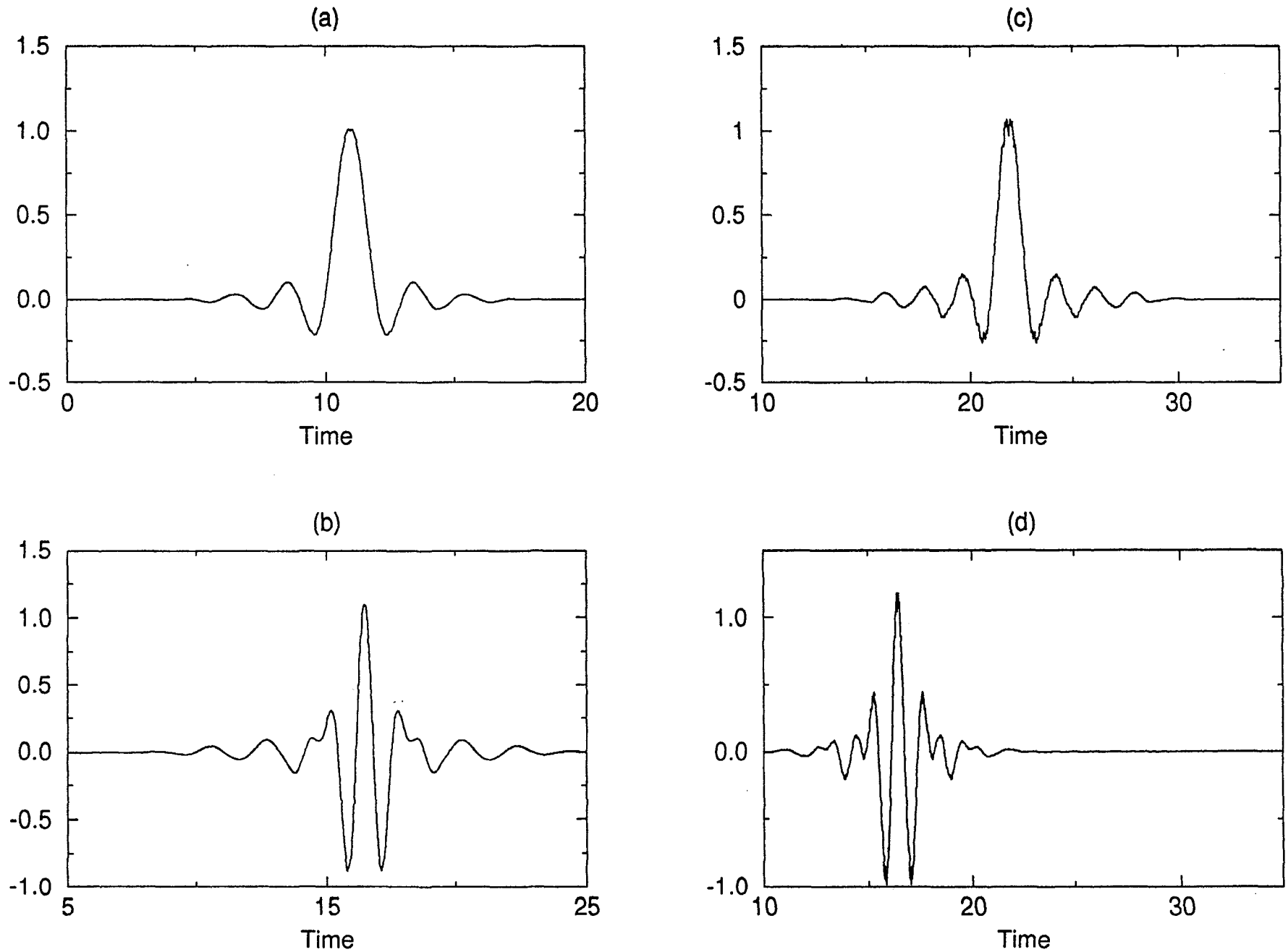

Fig. 4.5. (Example 4.2(i)) The symmetric limit functions generated by using the FIR filter bank in Example 3.2 ($H_0(z)$ has 2 zeros at π).
(a) Analysis scaling function. (b) Analysis wavelet function.
(c) Synthesis scaling function. (d) Synthesis wavelet function.

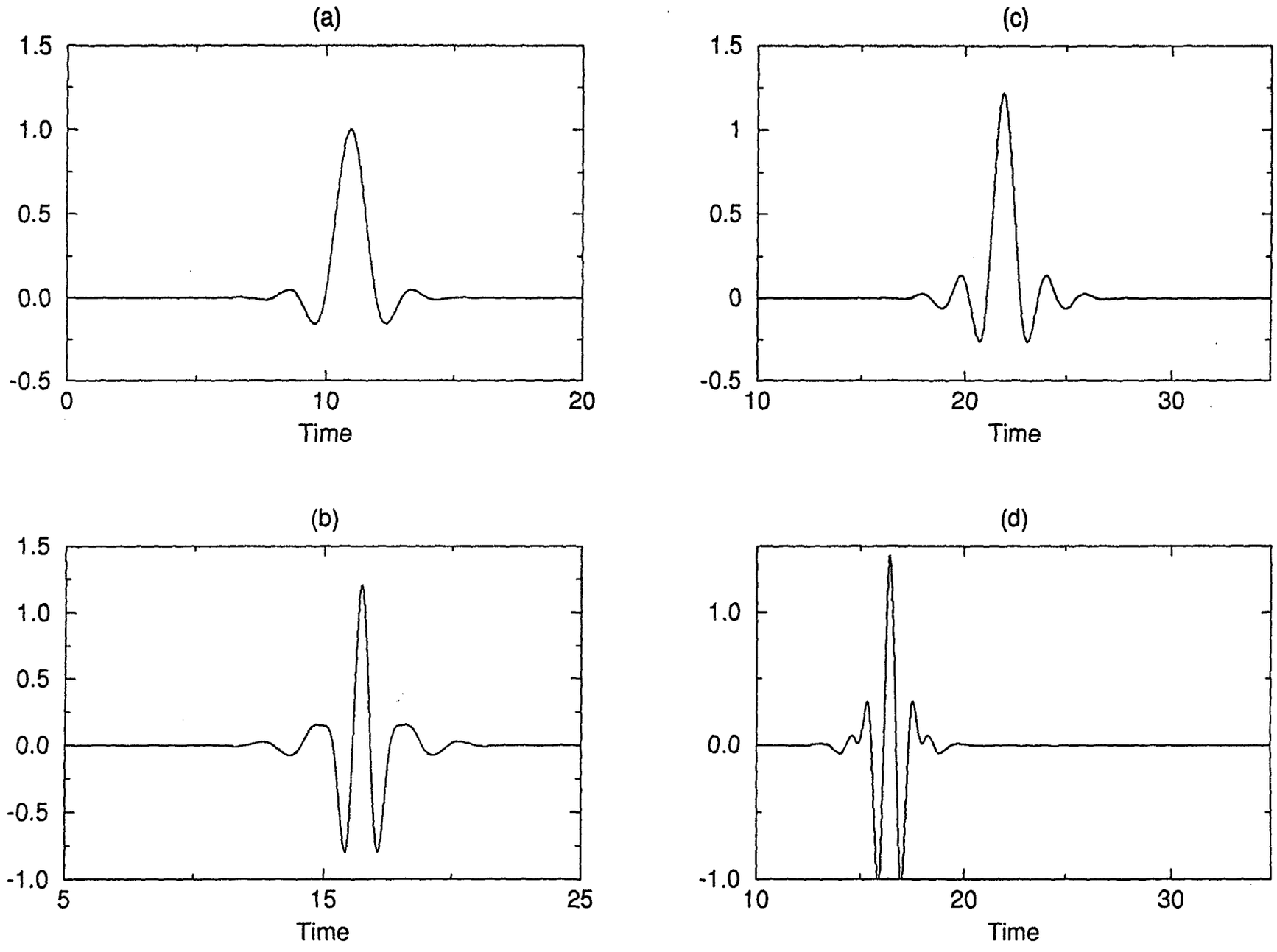

Fig. 4.6. (Example 4.2(ii)) The symmetric limit functions generated by using the FIR maximally flat filter bank ($H_0(z)$ has 12 zeros at π).
(a) Analysis scaling function. (b) Analysis wavelet function.
(c) Synthesis scaling function. (d) Synthesis wavelet function.

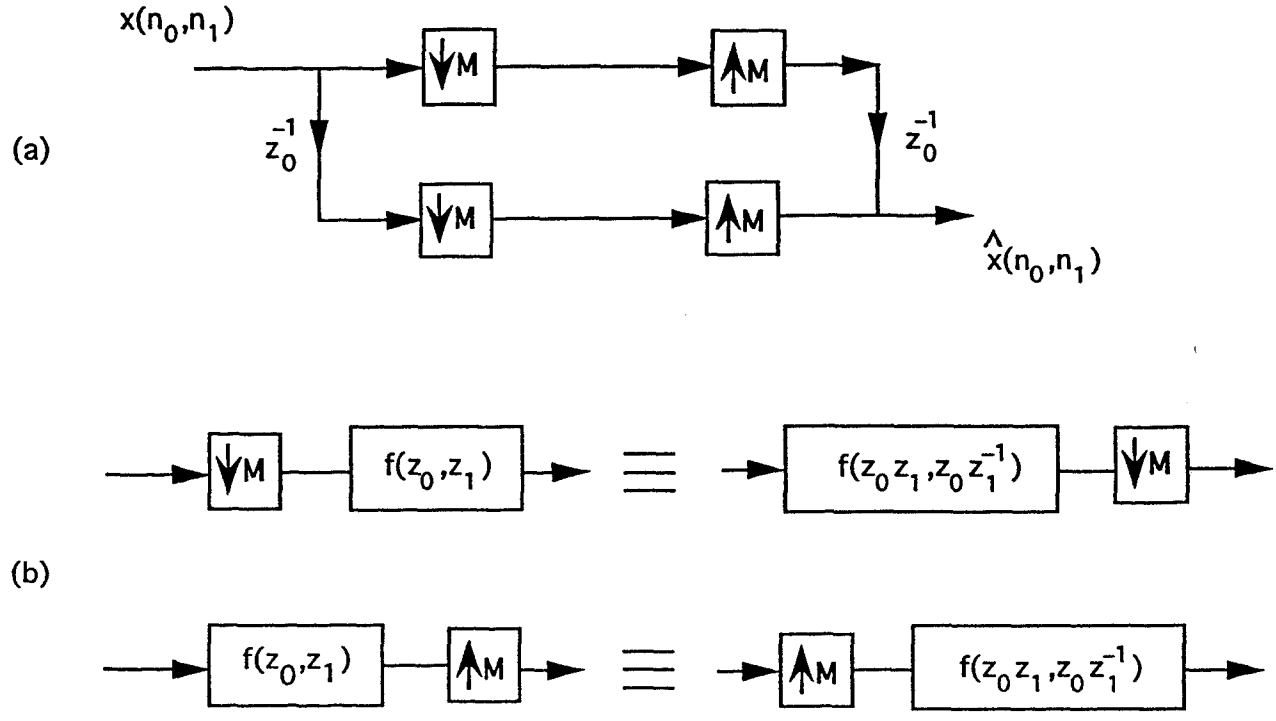

Fig. 5.3. Some details for the quincunx decimator
(a) The delay chain perfect reconstruction system, and
(b) the noble identities.

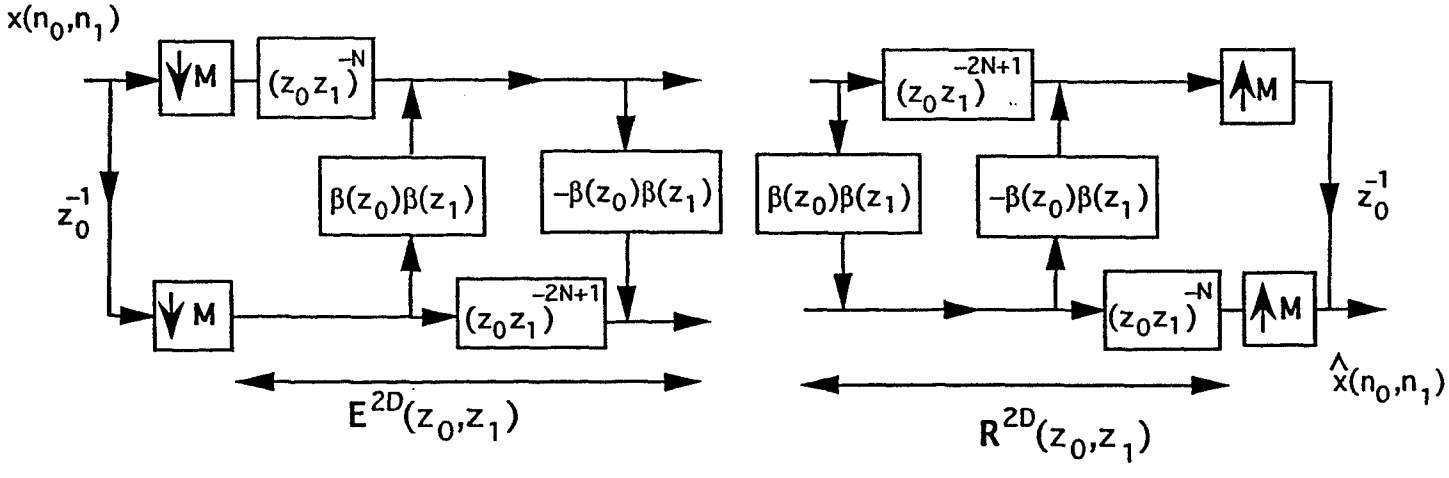

Fig. 5.4. A 2D biorthogonal filter bank obtained from Fig. 2.1 by mapping.

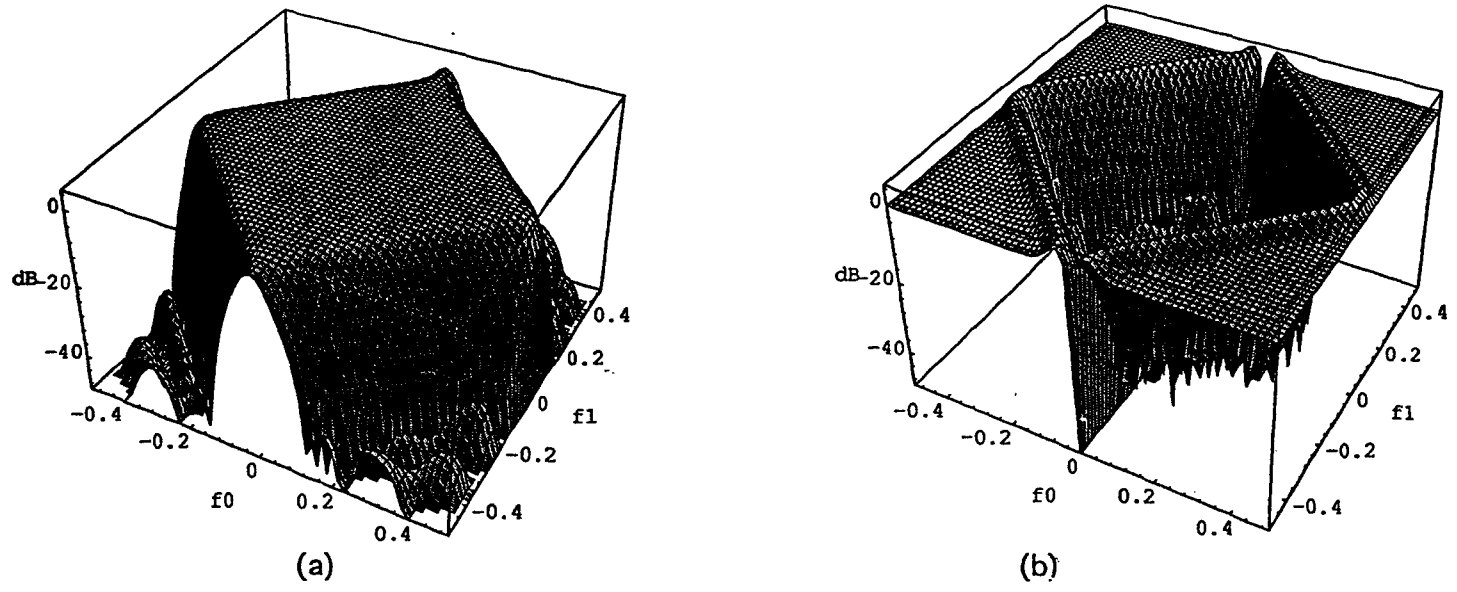

Fig. 5.5. (Example 5.1) Magnitude responses of the perfect reconstruction IIR analysis bank. (a) $H_0(z_0,z_1)$ and (b) $H_1(z_0,z_1)$. The normalized frequency $f_i=\omega_i/2\pi$.

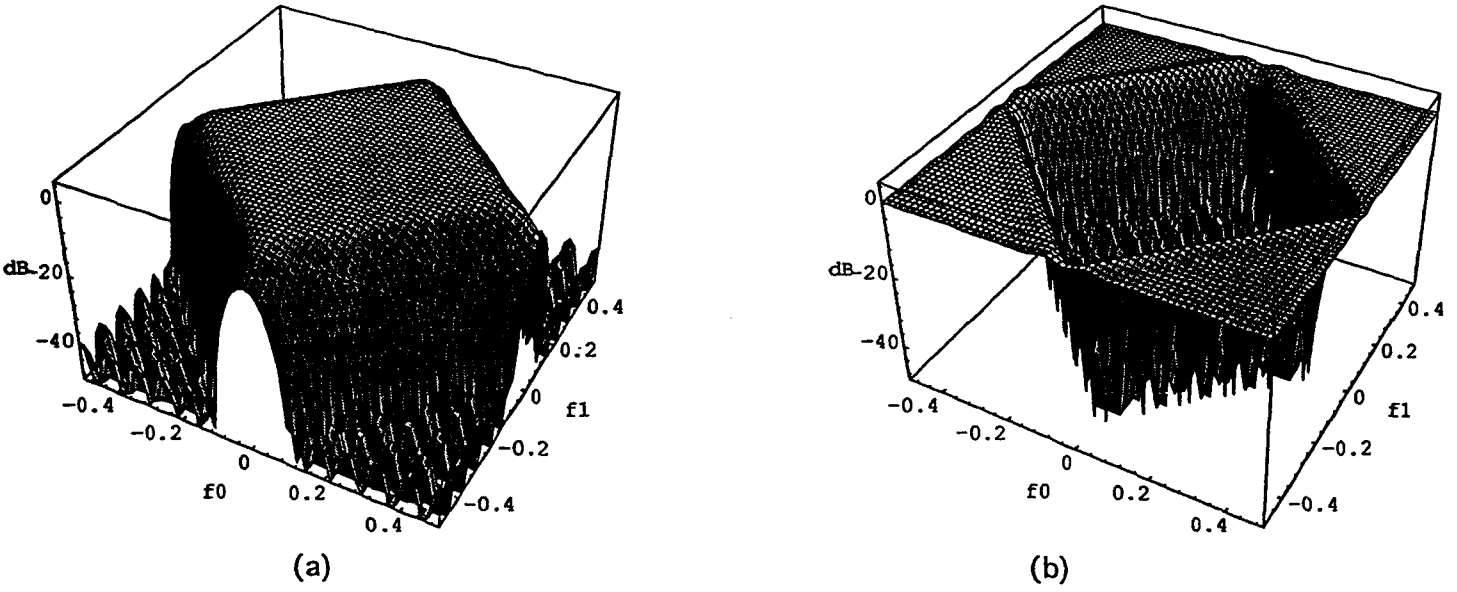

Fig. 5.6. (Example 5.2) Magnitude responses of the perfect reconstruction FIR analysis bank. (a) $H_0(z_0,z_1)$ and (b) $H_1(z_0,z_1)$.

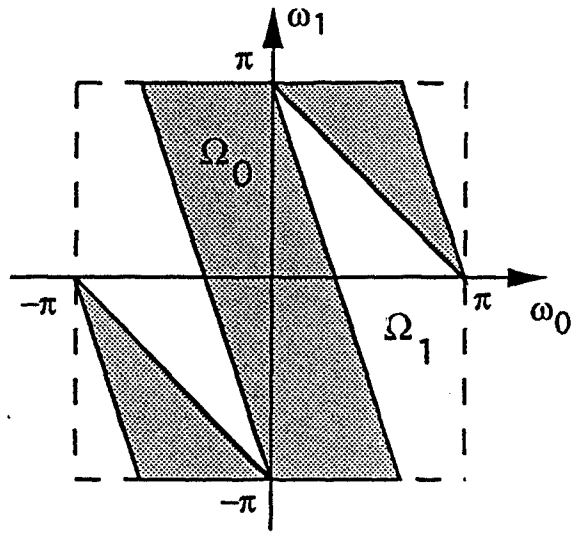

Fig. 6.1. The ideal supports for alias-free decimation with **M** defined in (6.1).

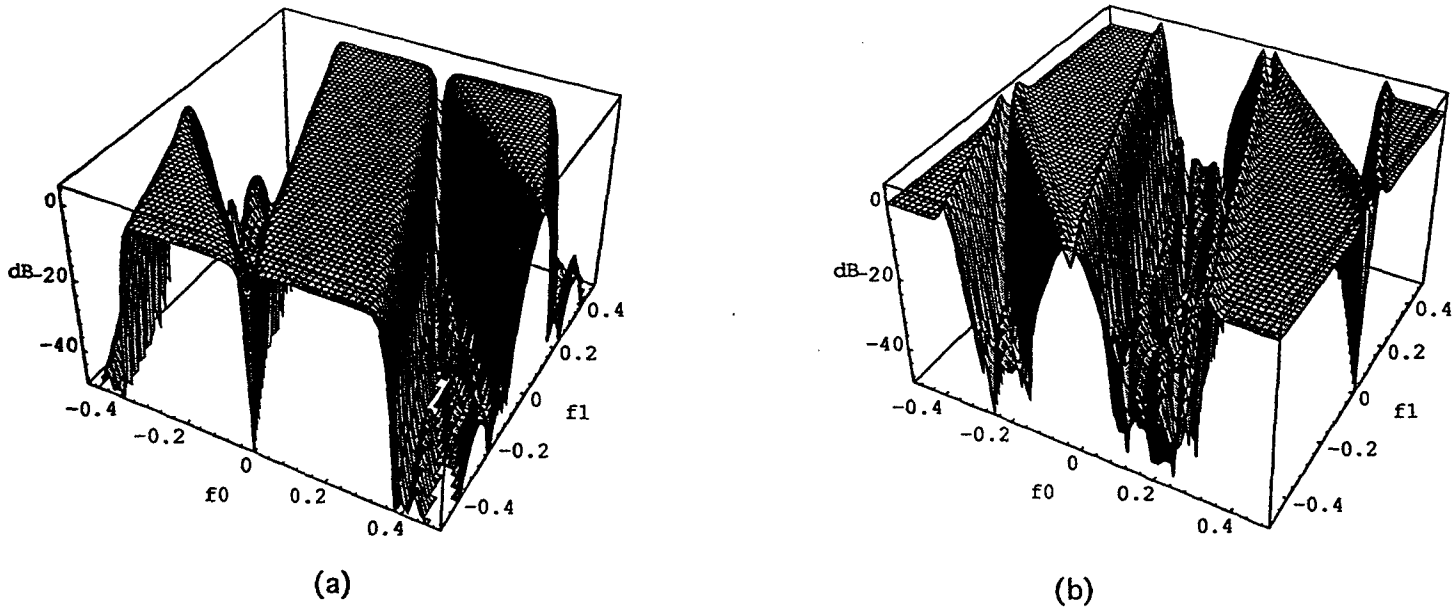

Fig. 6.2. (Example 6.1) Magnitude responses of the perfect reconstruction analysis bank with the decimator **M** defined in (6.1).
(a) $H_0(z_0,z_1)$ and (b) $H_1(z_0,z_1)$.

FOOTNOTES

1. Manuscript received

2. This work was supported by Office of Naval Research grant N00014-93-0231, and funds from Tektronix, Inc.

3. See-May Phoong and P. P. Vaidyanathan are with the Department of Electrical Engineering, California Institute of Technology, Pasadena, CA 91125.

4. Chai W. Kim is with Department of Electrical Engineering, University of Pennsylvania, 200 S. 33rd St., Philadelphia PA 19104 USA.

5. Rashid Ansari is with Bellcore MRE 2A-277, 445 South Street Morristown NJ 07960 USA.